國 立 交 通 大 學

工學院專班精密與自動化學程

碩 士 論 文

離心滾磨機的動態分析

Dynamic Analysis of the Centrifugal Crushing Machine

研 究 生：彭星雲

指導教授：成維華　教授

中華民國九十八年二月

離心滾磨機的動態分析

Dynamic Analysis of the Centrifugal Crushing Machine

研　　究　　生：彭星雲　　Student：Sing-Yun Peng

指　導　教　授：成維華 博士　　Advisor：Dr.Wei-Hua Chieng

國 立 交 通 大 學

工學院專班精密與自動化學程

碩 士 論 文

A Thesis

Submitted to Degree Program of Automation and Precision Engineering

College of Engineering

National Chiao Tung University

in Partial Fulfillment of the Requirements

for the Degree of

Master of Science

in

Automation and Precision Engineering

February 2009

Hsinchu, Taiwan, Republic of China

中華民國九十八年二月

離心滾磨機的動態分析

研究生:彭星雲　　指導教授:成維華 教授

國立交通大學工學院專班精密與自動化學程

摘　要

現今奈米等級合金的材料越來越多使用了，主要是一般合金材料研磨到奈米等級時，其物理性質會有不一樣現象，對於現今的科學很有幫助，因此如何將一般的合金材料研磨成奈米等級，是重要的技術,現今一般的物理性的研磨機，最主要的問題就是在研磨時會產生熱量，對研磨機及研磨粉末都不好的影響, 需要額外的方法及成本, 將熱量帶出或減少，因此在此前提下, 研發出新的研磨機，是以行星式的方式設計其研磨機，研磨機上有研磨槽可將需要研磨顆粒放入，且研磨槽內有一研磨棒，當機台運動時，研磨槽會產生自轉及公轉，而研磨棒會在研磨槽內滾動且會產生的離心力，其離心力可以壓碎顆粒，達成研磨的效果。

Dynamic Analysis of the Centrifugal Crushing Machine

Student : Sing-Yun Peng Advisor : Dr. Wei-Hua Chieng

Automation and Precision Engineering
College of Engineering
National Chiao Tung University

Abstract

Recently, a growing number of the engineering applications require the material of Nano-scale alloy. The main reason is that the physical property would be different when the normal alloy material is mill grinded into Nano-scale powder which is useful for current science. The most important skill is that how to grind the general alloy material into Nano-scale. For the current normal physical grinder the main problem is that grinding generates heat which has negative effect for grinder and powders. Additional methodology and cost are required to reduce or bring out the heat. For this reason, a new grinder with the planetary design is developed. The grinder has a cup with a hammer and the granule could be put in it. When the grinder is working, there is the rotation and revolution motion in the cup. The hammer is rolling in the cup and generating centrifugal force and then crumbling these granules.

誌謝

首先誠摯的感謝指導教授成維華博士, 三年來老師的悉心指導, 並不時的討論與指點我正確的方向, 使我在這段求學的時間獲益良多。老師對學問的嚴謹態度更是我們學習的典範。

三年的日子說長不長, 說短還真短, 一眨眼就過了。這段時間在一邊工作又一邊在學校讀書, 說實在真的很累尤其工作上常常會有不定時的意外, 造成更多的工作量, 常常會有學業與工作的抉擇, 這次在職專的求學, 可能是人生中最後一段求學的日子, 感謝實驗室的學長學弟以及同學們, 這段回憶因為有你們而令人難忘。

感謝黑人、葛雷學長在我遇到研究的困難時, 總能適時的伸出援手, 討論並指引我方向, 給我莫大的助益, 尤其黑人學長幫助我最大, 在此最謝謝他, 還有本屆的同學學磊、富源哥, 謝謝你們的支持與我共同完成這學業。

最後, 謹以此文獻給在求學的路上無條件支持我的父母。

Contents

List of Tables

List of Figures

Chapter 1 Introduction

1.1 Nano-powder

Nano-material is powder, fiber, membrane or clot in Nano-scale. By science verification, to process normal materials to get in Nano-scale accompanies peculiar effect upon surface, volume or quantum and accordingly arises distinct changes in optics, calorifics, electricity, magnetics, mechanics and even chemical character. In consequence, Nano-materials have superior character which is not ubiquitous in general materials and can be extensively applied to various fields as the electron, the medicine, the chemical industry, the military, Aero-Space, etc. Overall, nano-material can be categorized as nano-power, nano-fiber, nano-membrane and nano-clot. Among others, Nano-powder which has the longest research and the developed technology is the foundation of the other three nano-materials. Nano-powder also known as ultra little powder or ultra thin powder is powder or pellet whose size is under 100 nano-scale. It is one kind of the solid particle material among atom, molecule and object. Nano-powder is adopted in the high density magnetic storage materials, the wave-absorbing materials, the Solar Cell materials, the high-effective catalytic or the high-effective combustion improver.

1.2 Nano-powder of mode of production

The mode to produce nano-powder is divided into physical method and chemical method. The physical method of product nano-powder includes ball-milling method, gas condensation method, physical smashing

method, thermal decomposition method and Supercritical Fluid method. The chemical method includes Chemical Vapor Deposition, micro-emulsion method, polymer graftage method, sol-gel process method, chemical precipitation method, Hydrothermal Synthesis method, etc.

Up to present, unit nano-powder could be obtained by chemical method, inasmuch as chemistry nano-powder production has been massively researched and been provided plenteous harvests. However, mostly the cost of chemical method is quite high and no much space to be reduced. In addition, the caliber of nano-powder produce by chemical method is larger than the one by physic. Consequently, nano-powder is mostly produce by physical machinery mill.

Physical machinery mill is a usual and accepted method to produce much nano-powder in industry field. Chemistry nano-powder production even could make unit nano-scale powder and also bigger caliber nano-powder inasmuch as it has massive research and plenteous harvest. However, most of the production cost by chemical method is quite higher than which by physical machinery mill and very hard to be reduced. On the contrary, machinery mill could take lower production cost to extract nano-powder with similar caliber each. The parameters of physical machinery mill are apt to be controlled to magnify upon mass production machines. Up to present, physical machinery could produce 30nm powder only; nevertheless, it is enough to meet the market demand.

Machinery mill is to use the share force, friction and momentum to squash pellets from bigger to smaller. Obviously, the friction force would bring pellets enormous energy and accelerate its temperature raised rapidly. Further, how to avoid dust storm problem as the pellets get smaller is also

the essential of the production of physical machinery mill. Therefore, most mill machine is designed some specification to channelize heat, for instance, to fill nitrogen, but it would increase the cost simultaneously.

1.3 Ball mill machine

A ball mill, a type of grinder, is a cylindrical device used in mill (or mixing) materials like ores, chemicals, ceramic raw materials and paints. Ball mills rotate around a horizontal axis, partially filled with the material to be ground plus the mill medium. Different materials are used as media, including ceramic balls, flint pebbles and stainless steel balls. An internal cascading effect reduces the material to a fine powder. Industrial ball mills can operate continuously, fed at one end and discharged at the other end. Large to medium-sized ball mills are mechanically rotated on their axis, but small ones normally consist of a cylindrical capped container that sits on two drive shafts (pulleys and belts are used to transmit rotary motion). A rock tumbler functions on the same principle. Ball mills are also used in pyrotechnics and the manufacture of black powder, but cannot be used in the preparation of some pyrotechnic mixtures such as flash powder because of their sensitivity to impact. High-quality ball mills are potentially expensive and can grind mixture particles to as small as 0.0001 mm, enormously increasing surface area and reaction rates. The mill works on principle of critical speed. The critical speed can be understood as that speed after which the steel balls which are responsible for the mill of particles starts rotating along the direction of the cylindrical device; thus cause no mill further.

1.4 Planetary ball mill machine

In order to reduce or eliminate the generation of thermal energy and avoid any friction force or momentum in mill, it must be supposed to make any new idea in mill. Refer to Figure 1.1, to mill by hammer as the car motion to scrunch pellets by wheel rolling is the foundation. As to change the weight of car, the heavy the car's weight is the much the power will get to crush pellets. Furthermore, wheel takes the rolling motion on a smooth road and does not produce any friction force and momentum. The planetary ball mill machine is designed by the idea. Planetary mill machine is mainly composed of three mechanisms which are one solar gear wheel, one arm and three planetary gear wheels. In Figure 1.4,every planetary gear wheel connects with the arm. Every mill cup has a mill hammer. When the solar gear wheel and the arm rotate, the three planetary gear wheels do synchronously rotation and revolution. Then, the mill cup on the planetary gear wheel rotates accordingly. The mill hammer also pivots by the mill cup rotation. The mill hammer moves like the wheel of car and rolls around in the mill cup to crush pellets. Consequently. The design of the arm of planetary mill machine brings the huge force similar to the power of the wheel from the weight of car can mash the pellets to powder.

In Figure 1.5, the planetary ball mill machine rolls in the mill cup as the wheel of car moves on the smooth road. In Figure 1.5, like the move of car wheel on a smooth road, supposing the planetary ball mill machine ceaselessly rolls around the inner wall of the mill cup and doesn't produce friction force, it amounts little thermal energy. In addition, the size of the grinded powder can be control by the rolling of planetary mill machine as

the positive power can be bridled by the rolling speed of solar gear wheel and arm. The above are the purposes of the designed the planetary ball mill machine which could grind pellets to nano-scale powder.

Chapter 2 Derivation of equation of the planetary ball mill machine

Rotary table is attached to the arm. The mill cup is attached to the planetary gear. The mill hammer moves on the rotary table within the mill cup. Assuming no friction force presents on the interface between the rotary table and the grinder. In Figure 2.1, Point Q, on the mill cup, is the intersection point between the inner surface of the cup and the extension line between center of the mill hammer and the mill cup, Point B, on the mill hammer, is the intersection point between the outer surface of the hammer and the extension line between center of the mill hammer and the mill cup.

Define position vector $\vec{r} = \overrightarrow{AH}$.

The unit vector $\vec{u}$ is defined as that $\vec{u} = \frac{\vec{r}}{r}$.

Position vector $\vec{r}_A = \overrightarrow{OA}$.

The inner radius of the mill cup is denoted by r_C.

The radius of the cylindrical grinder is denoted by r_H.

The distance between A and H is denoted by r.

The unit vector $\vec{k}$ is along the z-axis.

The position vector of point Q is $\vec{r}_Q = \overrightarrow{OQ} = \vec{r}_A + r_C\vec{u}$.

The position vector of center of the grinder is $\vec{r}_H = \overrightarrow{OH} = \vec{r}_A + \vec{r}$.

The position vector of point B is

$$\vec{r}_B = \overrightarrow{OB} = \vec{r}_H + r_H\vec{u}\ \vec{r}_{B/Q} = \vec{r}_B - \vec{r}_Q = \vec{r} + r_H\vec{u} - r_C\vec{u} = (r + r_H - r_C)\vec{u}$$

The velocities are

$$\vec{v}_Q = \frac{d\vec{r}_Q}{dt} = \frac{d\vec{r}_A}{dt} + r_C \frac{d\vec{u}}{dt} = \omega_A \vec{k} \times \vec{r}_A + r_C(\omega_P + \omega_A)(\vec{k} \times \vec{u}) \quad (2\text{-}1)$$

$$\vec{v}_H = \frac{d\vec{r}_H}{dt} = \frac{d\vec{r}_A}{dt} + \frac{dr}{dt}\vec{u} + r\frac{d\vec{u}}{dt} = \omega_A \vec{k} \times \vec{r}_A + \frac{dr}{dt}\vec{u} + r(\omega + \omega_A)(\vec{k} \times \vec{u})$$

$$\vec{v}_B = \vec{v}_H + r_H \frac{d\vec{u}}{dt} = \vec{v}_H + r_H(\omega_H + \omega_A)(\vec{k} \times \vec{u}) \quad (2\text{-}2)$$

$$\vec{v}_{B/Q} = \vec{v}_B - \vec{v}_Q = \frac{dr}{dt}\vec{u} + (r\omega + r_H\omega_H - r_C\omega_P + (r + r_H - r_C)\omega_A)(\vec{k} \times \vec{u}) \quad (2\text{-}3)$$

The accelerations are

$$\vec{a}_Q = \frac{d\vec{v}_Q}{dt} = \omega_A \vec{k} \times (\omega_A \vec{k} \times \vec{r}_A) + \alpha_A \vec{k} \times \vec{r}_A + r_C(\alpha_P + \alpha_A)(\vec{k} \times \vec{u}) + \quad (2\text{-}4)$$

$$+ r_C(\omega_P + \omega_A)^2(\vec{k} \times (\vec{k} \times \vec{u}))$$

$$\vec{a}_H = \frac{d\vec{v}_H}{dt} = \omega_A \vec{k} \times (\omega_A \vec{k} \times \vec{r}_A) + \alpha_A \vec{k} \times \vec{r}_A + \frac{d^2r}{dt^2}\vec{u} + 2\frac{dr}{dt}(\omega + \omega_A)(\vec{k} \times \vec{u}) \quad (2\text{-}5)$$

$$+ r(\alpha + \alpha_A)(\vec{k} \times \vec{u}) + r(\omega + \omega_A)^2(\vec{k} \times (\vec{k} \times \vec{u}))$$

$$\vec{a}_B = \vec{a}_H + r_H(\alpha_H + \alpha_A)(\vec{k} \times \vec{u}) + r_H(\omega_H + \omega_A)\ (\vec{k} \times (\vec{k} \times \vec{u})) \quad (2\text{-}6)$$

$$\vec{a}_{B/Q} = \vec{a}_B - \vec{a}_Q = (r(\alpha + \alpha_A) + r_H(\alpha_H + \alpha_A) - r_C(\alpha_P + \alpha_A) + \quad (2\text{-}7)$$

$$2\frac{dr}{dt}(\omega + \omega_A))(\vec{k} \times \vec{u}) + \frac{d^2r}{dt^2}\vec{u} + (r(\omega + \omega_P)^2 + r_H(\omega_H + \omega_A)^2$$

$$- r_C(\omega_P + \omega_A)^2)(\vec{k} \times (\vec{k} \times \vec{u}))$$

2.1 Contact Motion

In Figure 2.2

$$r = r_C - r_H \qquad \frac{dr}{dt} = 0 \qquad \frac{d^2r}{dt^2} = 0 \quad (2\text{-}8)$$

$$\vec{v}_{B/Q} = (r\omega + r_H\omega_H - r_C\omega_P)(\vec{k} \times \vec{u}) \quad (2\text{-}9)$$

Knowing that

$$\vec{a}_H = \vec{a}_{H,N} + \vec{a}_{H,F} \qquad (2\text{-}10)$$

where

$$\vec{a}_{H,N} = r(\omega + \omega_A)^2 + \omega_A{}^2 r_A \cos\theta - \alpha_A r_A \sin\theta \qquad (2\text{-}11)$$

$$\vec{a}_{H,F} = r(\alpha + \alpha_A) + \omega_A{}^2 r_A \sin\theta + \alpha_A r_A \cos\theta \qquad (2\text{-}12)$$

The force equilibrium yields that

$$N = m\vec{a}_{H,N} \qquad (2\text{-}13)$$

$$F = m\vec{a}_{H,F} \qquad (2\text{-}14)$$

The above equations are provided with the assumption that

$$\vec{a}_{H,N} \geq 0 \qquad (2\text{-}15)$$

Moment equilibrium about point H yields that

$$r_H(ma_{H,F}) = I(\alpha_H + \alpha_A) \qquad (2\text{-}16)$$

where the moment of inertia of the mill hammer I is

$$I = Jmr_H^2 \qquad (2\text{-}17)$$

which yields that

$$r(\alpha + \alpha_A) + \omega_A{}^2 r_A \sin\theta + \alpha_A r_A \cos\theta - Jr_H(\alpha_H + \alpha_A) = 0 \qquad (2\text{-}18)$$

Or $$\alpha_H = \frac{r\alpha + (r + r_A\cos\theta - Jr_H)\alpha_A + \omega_A{}^2 r_A \sin\theta}{Jr_H} \qquad (2\text{-}19)$$

Let $r_C = \beta r_A$ And $r_H = \zeta r_A$ (2-20)

It is obtained that

$$r = (\beta - \zeta) r_A \qquad (2\text{-}21)$$

Eq.(2-18) may be rewritten as

$$\alpha_H = \frac{(\beta-\zeta)\alpha + ((\beta-\zeta)+\cos\theta - J\zeta)\alpha_A + \omega_A{}^2 \sin\theta}{J\zeta} \quad (2\text{-}22)$$

Let $\tilde{\tilde{a}}_{H,N}$ and $\tilde{\tilde{a}}_{H,F}$ denote the normalized accelerations due to r_A that $\tilde{\tilde{a}}_{H,N} = \vec{a}_{H,N} / r_A$, $\tilde{\tilde{a}}_{H,F} = \vec{a}_{H,F} / r_A$, they can be written as follows:

$$\tilde{\tilde{a}}_{H,N} = (\beta-\zeta)(\omega+\omega_A)^2 + \omega_A{}^2 \cos\theta - \alpha_A \sin\theta \quad (2\text{-}23)$$

$$\tilde{\tilde{a}}_{H,F} = (\beta-\zeta)(\alpha+\alpha_A) + \omega_A{}^2 \sin\theta + \alpha_A \cos\theta \quad (2\text{-}24)$$

2.1.1 Rolling motion

$$\vec{v}_{B/Q} = 0 \quad (2\text{-}25)$$

$$\omega = \frac{r_C\omega_P - r_H\omega_H}{r} = \frac{\beta\omega_P - \zeta\omega_H}{\beta-\zeta} \quad (2\text{-}26)$$

Assuming that the rolling motion remains, the acceleration may be derived by taking derivative to the above equation as follows:

$$\alpha_H = \frac{r_C\alpha_P - r\alpha}{r_H} = \frac{\beta\alpha_P - (\beta-\zeta)\alpha}{\zeta} \quad (2\text{-}27)$$

Substituting the above equation into Eq. (54) into Eq. (3), we obtain

$$\begin{aligned}\alpha = \ddot{\theta} &= \frac{Jr_C\alpha_P - (r + r_A\cos\theta - Jr_H)\alpha_A - \omega_A{}^2 r_A \sin\theta}{(1+J)r} \\ &= \frac{J\beta\alpha_P - (\beta-\zeta-J\zeta+\cos\theta)\alpha_A - \sin\theta\omega_A{}^2}{(1+J)(\beta-\zeta)}\end{aligned} \quad (2\text{-}28)$$

The rolling motion must be assured by the required friction force $F = m\vec{a}_{H,F}$ must be less than $\mu_S m\vec{a}_{H,N}$ which equates that

$$\tilde{\tilde{a}}_{H,F} = (\beta - \zeta)(\alpha + \alpha_A) + \omega_A{}^2 \sin\theta + \alpha_A \cos\theta \le \mu_S \tilde{\tilde{a}}_{H,N} \qquad (2\text{-}29)$$

2.1.2 Sliding motion

When Eq.(2-29) failed, we have

$$\mu_k N = m\vec{a}_{H,F} \qquad (2\text{-}30)$$

or $$\pm \mu_k \tilde{\tilde{a}}_{H,N} = (\beta - \zeta)(\alpha + \alpha_A) + \omega_A{}^2 \sin\theta + \alpha_A \cos\theta$$

The sign in front of $\mu_k \tilde{\tilde{a}}_{H,N}$ depends on the direction of the normalized slip velocity $\tilde{v}_{slip}$ which is defined that

$$\tilde{v}_{slip} = \frac{v_{B/Q}}{r_A} = \frac{r\omega + r_H \omega_H - r_C \omega_P}{r_A} = (\beta - \zeta)\omega + \zeta\omega_H - \beta\omega_P \qquad (2\text{-}31)$$

When $\tilde{v}_{slip} > 0$, we have

$$\alpha = \frac{-\mu_k \tilde{\tilde{a}}_{H,N} - (\beta - \zeta + \cos\theta)\alpha_A - \sin\theta\omega_A{}^2}{(\beta - \zeta)} \qquad (2\text{-}32)$$

When $\tilde{v}_{slip} < 0$, we have

$$\alpha = \frac{\mu_k \tilde{\tilde{a}}_{H,N} - (\beta - \zeta + \cos\theta)\alpha_A - \sin\theta\omega_A{}^2}{(\beta - \zeta)} \qquad (2\text{-}33)$$

2.2 Steady State Analysis for Constant ω_S and ω_A

$$\ddot{\theta} + A\sin(\theta + \theta_A) = B \qquad (2\text{-}34)$$

$$A = \frac{\sqrt{\alpha_A{}^2 - \omega_A{}^4}}{(1+J)(\beta - \zeta)} \qquad (2\text{-}35)$$

$$B = \frac{J\beta}{(1+J)(\beta - \zeta)}(\alpha_P + \alpha_A) - \alpha_A \qquad (2\text{-}36)$$

$$\theta_A = \tan^{-1}\frac{\alpha_A}{\omega_A{}^2} \qquad (2\text{-}37)$$

Subjected to constant inputs, i.e. $\alpha_P = \alpha_A = 0$, Eq.(61) becomes

$$\ddot{\theta} + A\sin\theta = 0 \qquad (2\text{-}38)$$

where

$$A = \frac{\omega_A{}^2}{(1+J)(\beta-\zeta)} \qquad (2\text{-}39)$$

The above equation is in form of a simple pendulum consists of a unit mass hanging from a string of length L (= g / A) and fixed at a pivot point P. The simple pendulum is displaced to an initial angle and released, the pendulum will swing back and forth with periodic motion. The frequency of the periodic motion is approximately

$$frequency = \sqrt{A} = \frac{\omega_A}{\sqrt{(1+J)(\beta-\zeta)}} \qquad (2\text{-}40)$$

The nonlinear equation may also be written as the energy form as follows

$$\frac{1}{2}\left(L\dot{\theta}\right)^2 + gL(1-\cos\theta) = \frac{1}{2}\dot{\theta}^2 + A(1-\cos\theta) = \text{constant} \qquad (2\text{-}41)$$

The solution is obtained that

$$\dot{\theta} = \pm\sqrt{\dot{\theta}_0{}^2 + 2\frac{\omega_A{}^2(\cos\theta - \cos\theta_0)}{(1+J)(\beta-\zeta)}} \qquad (2\text{-}42)$$

where θ_0 and $\dot{\theta}_0$ are initial angular position and velocity respectively. Solution from Eq.(2-42) can be more efficient and accurate than that from Eq. (2-38) during the numerical analysis. The crushing force N is proportional to the normalized normal acceleration.

$$N \propto \tilde{\tilde{a}}_{H,N} = (\beta - \zeta)(\omega + \omega_A)^2 + \omega_A{}^2 \cos\theta \qquad (2\text{-}43)$$

2.2.1 Finite Swing Crushing

Since the terms within the square root in Eq.(2-38) must be non-negative,

$$\dot{\theta}_0{}^2 + 2\frac{\omega_A{}^2(\cos\theta - \cos\theta_0)}{(1+J)(\beta - \zeta)} \geq 0 \qquad (2\text{-}44)$$

it is possible to evaluate the maximum swing at the zero angular velocity , i.e. $\dot{\theta} = 0$, as follows:

$$\theta_{\max} = \cos^{-1}(\cos\theta_0 - (1+J)(\beta - \zeta)\frac{\dot{\theta}_0{}^2}{2\omega_A{}^2}) \qquad (2\text{-}45)$$

2.2.2 Continuous Rotation Crushing

Instead of finite swing, the mill-hammer will continuously make 360° rotation when Eq. (2-45) failed to reach a solution, i.e.

$$\left(\frac{\dot{\theta}_0}{\omega_A}\right)^2 > 2\frac{\cos\theta_0 + 1}{(1+J)(\beta - \zeta)} \qquad (2\text{-}46)$$

In order to reach continuous rotation crushing, the slip velocity must be sustained till reaches -180° at the initial acceleration stage.

$$\tilde{v}_{slip} = (\beta - \zeta)\omega + \zeta\omega_H - \beta\omega_P < 0, \text{ for } . > \text{-}180^\circ \qquad (2\text{-}47)$$

or

$$\omega_P > \frac{(\beta - \zeta)\omega + \zeta\omega_H}{\beta}, \text{ for } . > \text{-}180^\circ \qquad (2\text{-}48)$$

The critical condition for continuous rotation crushing is that the roll motion starts at θ_0 = -180° and according to Eq.(2-42), it is written as

$$\omega = \frac{\beta\omega_P - \zeta\omega_H}{\beta - \zeta} = 0 \text{, for } \theta = \theta_0 = -180^0 \qquad (2\text{-}49)$$

or

$$\omega_H = \frac{\beta}{\zeta}\omega_P \text{, for } \theta = \theta_0 = -180^0 \qquad (2\text{-}50)$$

2.3 Equation of Torque

In Figure 2.3.

The torque equilibrium equation subjected to the arm is

$$\tau_A = I_A\alpha_A + m_P r_A^{\,2}\alpha_A + \vec{F}_Q \times \vec{r}_A + \tau_P \qquad (2\text{-}51)$$

The torque of each planet may be derived from the equilibrium equation as follows:

$$\tau_P = I_P(\alpha_P + \alpha_A) + \vec{F}_Q \times (\vec{r}_Q - \vec{r}_A) \qquad (2.52)$$

Where $\vec{F}_Q$ is perpendicular to $\vec{r}_Q - \vec{r}_A$, of which the magnitude is

$$\left|\vec{F}_Q\right| = \mu m_H \left|\vec{a}_{H,N}\right| = \mu m_H \left\{r(\omega + \omega_A)^2 + \omega_A^{\,2} r_A \cos\theta - \alpha_A r_A \sin\theta\right\} \qquad (2.53)$$

There are two servo motor assembling the planetary ball mill machine. One servo motor is assembling the arm and the other is assembling the solar gear wheel. And the torque of servo motor is controlled by the electric current. The equation is written as

I_E = electric current K=coefficient

$$KI_E = \tau \qquad (2.54)$$

So it can be as

$$KI_{EA} = \tau_A = I_A \alpha_A + m_p r_A^{\ 2} \alpha_A + \vec{F}_Q \times \vec{r}_A + \tau_P \tag{2.55}$$

$$KI_{EP} = \tau_P = I_P(\alpha_P + \alpha_A) + \vec{F}_Q \times (\vec{r}_Q - \vec{r}_A) \tag{2.56}$$

2.4 Velocity Planning

There are two d.o.f. (degrees-of-freedom) to be controlled. Without loss of generality, we choose the velocities ω_A and ω_P as the inputs. The practical velocity input may be

$$\omega_A = \begin{cases} \alpha_A t & \text{when } t \le T_a \\ \alpha_A T_a & \text{when } t > T_a \end{cases}$$

$$\omega_P = \begin{cases} \alpha_P t & \text{when } t \le T_a \\ \alpha_P T_a & \text{when } t > T_a \end{cases}$$

providing that α_A and α_P are distinct constant accelerations.

Chapter 3 Frame of experiment

3.1 Hardware of experiment

There are four apparatus to make up the planetary ball mill machine. The first part is the arm. Such as Figure 3.1. There is the model V belt pulley which is set up under the arm. The second part is the planetary wheel which is called the cup, too. The inside wall of the cup is smooth. The Roughness of the inside wall for the cup is lower than 1 μm. There is the gear which is set up under the cup. Such as Figure 3.2. There are three the planetary cup to make up the solar wheel with gear wheel. The third part is the two motors which is divided into the motor A and the motor B. It is specification is like table3.1. Because the angular velocity of the arm and the angular velocity of the cup are controlled, we select the servo motor. In addition, the inertia of the cup and the inertia of the arm are larger. So we select the servo motor which surpass in 750W. In addition, we don't use the moderating machine to dives the arm and the cup. Because the power is lost by the moderating machine. The motor A drives the arm with the model V belt. The direct current of the power for the motor A is not to measure and the angular velocity of the arm is controlled steadily. So, the power of the motor is AC. And, the inertia of the motor which is AC servo motor is bigger. The motor B drives the cup with the shaft coupling. Such as Figure 3.3. Because the direct current of the power for the motor B is to measure, we select the DC servo motor. But, the horsepower the DC servo motor and the inertia of the DC servo are smaller. So, we select higher the watt of the DC servo motor. The fourth part is framework what is set up with the planetary ball mill machine. Such as Figure 3.4. The framework is

manufacture by five iron plate which welds each other. The framework needs to be heavy. Because, the planetary ball mill machine will be shaken when the planetary ball mill machine runs. Finally, there is one the hammer in every the cup. The function of the hammer is milled in the cup. This is just complete the planetary ball mill machine. Such as Figure 3.5. The surface of the hammer is very smooth. The roughness of the surface for the hammer is lower than 1 μm. And, the material of the hammer is should be heavy enough. The effect of the planetary ball mill machine will be a bit higher. Finally, we design and make the planetary ball mill machine. Such as Figure 3.6 and Figure 3.7.

In addition, there are two LED and the two LED are set up the top of hammer. The color of LED is red and white. There is one LED what is set up the side of the arm. The color of LED is yellow. There is one LED what is set up the side of the cup. The color of LED is blue. Such as Figure 3.6. And, there is a single-lens reflex camera what is set up the top of the planetary ball mill machine. Such as Figure 3.8. The locus of the four LED is taken by the camera shutter. And, the LED of the arm and the LED of the cup is auxiliary. We can determine the motion of the hammer with the locus of the LED for the hammer, the locus of the LED for the arm and the locus of the LED the cup.

3.2 Motion of the planetary ball mill machine

Because this is the planetary ball mill machine, we need to understand the motion of the planetary ball mill machine. First, in the Figure 3.9 , the sun gear assemble with the planetary gear and the planet gear set up the

arm. When the sum gear revolves, the planetary gear revolves on its own axis, too. When the arm revolves, the planet gear revolves on its own axis and revolves round the sun gear. In the Figure 3.9 , we define

ω_A = The angular velocity of arm.

ω_p = The angular velocity of the planetary gear.

ω_S = The angular velocity of the sun gear.

N_p = The teeth of the planetary gear.

N_S = The teeth of the sun gear.

r = the angular velocity ratio.

a = the pitch radius of the planetary gear.

b = the pitch radius of the sun gear.

V_c = the cutting velocity of the sun gear.

V_d = the cutting velocity of the sun gear.

In the Figure 3.9, if the sun gear revolves by oneself and the arm is fixed, we can find the velocity ratio r.

$$V_c = a\omega_P = b\omega_S \tag{3-1}$$

$a = 2\pi N_p$ and $b = 2\pi N_S$

$$r = -\frac{N_S}{N_P} = \frac{\omega_P}{\omega_s} \tag{3-2}$$

$$\omega_P = -\frac{N_S}{N_P}\omega_S \tag{3-3}$$

In the Figure 3.9, if the arm revolves by oneself and the sun gear is fixed, we can find the angular velocity of the planetary gear.

$$V_d = \omega_A(a+b) = V_c = \omega_p a \tag{3-4}$$

$$N_P\omega_P = \omega_A(N_P + N_S) \tag{3-5}$$

$$\omega_P = \omega_A(\frac{N_S}{N_P} + 1) \tag{3-6}$$

According to the equation 3-2 and the equation 3-4. When the sun gear and the arm revolve at the same time, the angular velocity of the planetary gear.

$$\omega_P = -\frac{N_S}{N_P}\omega_S + \omega_A(\frac{N_S}{N_P} + 1) \tag{3-7}$$

In the Figure3.10, the motor A drives the arm with the model V belt pulley and the model V belt. And, the radius of the model V belt pulley which is set up the motor A is r_1. The radius of the model V belt pulley which is set up the arm is r_2. We define

r_r = reduction ratio

$$r_r = \frac{r_1}{r_2} = 1 \tag{3-8}$$

According to the equation 3-8, the max angular velocity of the arm is 3000 rpm. And, the max angular velocity of the cup is 3000 rpm. Because the motor B drives the cup with the shaft coupling.

So, we can use the equation 3-8 and equation 3-7 to determine the angular velocity of the motor B.

3.3 Experiment setup

When the hardware of the planetary ball mill machine set up, we must select software to control the planetary ball mill machine. We must control

the angular velocity of the arm, the angular velocity of the cup and receive analogy single. So we select the HMI (human machine interface) which is WIN PC32. Such as Figure 3.10. WIN PC32 includes the motion module, the digital I/O module and the analogy I/O module. And, WIN PC32 is open PC-Based control. WIN PC32 is internationalized HMI software. So, the range of application for the WIN PC32 is quite extensive, such as Figure 3.11. So, WIN PC32 is easily to design interface, control the angular velocity of the arm and the angular velocity of the cup with the motion card and receive analogy with the AD/DA card. We select the specification of the PC, the motion card and the AD/DA card in the table 3.2.

We use Win PC32 to control the motor A and the motor B with PC and motion card. Such as Figure 3.12. The motion card is HAL 8506. HAL-8506 which is based on the EPCIO ASIC can provide 6 axes servo or stepping motor motion control with DDA (Digital Differential Analyzer) algorithm. The HAL-8506 has two operation modes: The first mode is to work with a velocity mode servo drive. The HAL-8506 compares the segmental movement commands from Host PC and the encoder feedback from servo motor, calculates, via P controls, the analog output command, then send the command to the velocity mode drive to control servo motor. The second mode is to convert the segmental movement command into well behaved, from frequency variance standpoint, pulse train and feed to either the use position mode servo drive or a stepper drive to control the motor. We write one HMI (Human Machine Interface) software to control the angular velocity of the motor A and the angular velocity the motor B. And, the motor A and the motor B are servo motor. The HMI software can receive the encode of the motors and determine the speed of the motor

which is rotating steadily. Such as Figure 3.13. At the same time, the HMI software can control the AD/DA card to record direct current of the power of the motor B at 10 ms. The AD/DA card is HAL-8184 which is designed to meet the requirement of general analog I/O with high speed counter board for half-size ISA Bus. HAL-8184 provides one isolated, 8 channels, 12 bits free-run analog inputs and 4 channels, 16 bits free-run analog output with 2 channels, 16 bits high speed counters. And the direct current of the power for the motor B is displaying the interface. Such as Figure 3.14. In Figure 3.13 is the circuit diagram which record direct current of the power for the motor B. The direct current is recorded with the Hall sensor. The Hall sensor is the LA 55-P. The LA 55-P can measure DC, AC, plused and mixed with a galvanic isolation between the primary circuit (high power) and the secondary circuit (electronic circuit).

The experiment is mainly to measure the torque of the motor which is changed by the normal force which is changed by the hammer which mill in the inside wall of the cup. According to the equation 2-55 and equation 2-56. When the torque of the motors are changed by external force, the direct current of the power for the motors are changed, too. So, we can measure the direct current of power for the motor A and the direct current for the motor B. But, when the planetary ball mill machine runs, the motor B dives the cup with the shaft coupling and the motor A dives the arm with the model V belt. So, it is right to record direct current of the power for the motor B. Because, the power of the motor A is lost by belt. The record needs to reach 10000 materials. Because , the request data of FFT need 10000 materials. So, we record the direct current of the power for the motors with AD/DA card. Finally, we use the record to transform frequency

with FFT. So, We can determine the specific of motion for the hammer is in the cup by the frequency of the direct current.

Finally, we can determine the effect of the planetary ball machine with the size of the powder. And the size of the powder is determined by the normal force of the hammer. The planetary ball machine must mill the size of the powder to reach nano grade. So, we must determine the motion of the planetary ball machine.

Chapter 4 To compare simulation analysis and the experimental data

4.1 Simulation analysis

We use visual C++ to design one simulation software with the equation in chapter 2. The simulation software can simulate the specific of motion for the hammer in the cup. And, the simulation software simulates the normal force of the hammer, the friction force of the hammer, ω and ω_H. We use the simulation software to simulate with the parameter in table 4.1 and the angular velocity in Figure 4.1. According to the simulation data, we can find the hammer which is in the cup has two motion. The first motion is the finite swing motion. The second motion is the continuous rotation motion.

In addition, we use visual C++ design another simulation software with the equation in chapter 2. The simulation software can simulate the specific locus of two side for the hammer, the specific locus of the cup and the specific locus of the arm. We use the simulation software to simulate with the parameter in table 4.1 and angular velocity in Figure 4.1.

4.1.1 Finite swing motion

When $\omega_A = 191.022$ rpm and $\omega_P = 286.533$ rpm , the motion of the hammer is the finite swing motion. The number of θ is among 12°～-12°. Such as Figure 4.2. We can use the equation 2-45 to prove θ which is right. The motion is the hammer which mill between 12°～-12° on inboard

wall of the cup. Such as Figure 4.3. The number of the normal force is among 27.5N～33.1N. Such as Figure 4.4. The number of normal force of the hammer can change the size of the powder. If the normal force of the hammer is bigger, the size of the powder is smaller . The number of the friction force is among 8.3N～10N. Such as Figure 4.5. The number of the friction force have relations with the number of the normal force. When the number of the normal force is greater, the number of the friction is greater, too. According to the equation 2-51 and the equation 2-52, we can find the torque to have relation with the friction. And, according to the equation 2-55 and the equation 2-56, we can find the direct current of the power to have relation with the torque. So, when the friction force is greater, the change of the direct current for the power is greater. ω is among -12rad/s～12rad/s. Such as Figure 4.6. According to the equation 2-23. When the ω is greater, the number of the normal force is greater, too. ω_H is among -42.5rad/s～-35.5rad/s. Such as Figure 4.7. According to the equation 2-26. When ω_H is greater, ω is greater, too. According to the equation 2.56. We can change from the torque to the direct current of power. K is coefficient of the motor B. So, the direct current of the power for the motor B is Figure 4.8. We must record 10000 data of direct current for the power every 10 ms. And, we can transform the direct current of power into the frequency with FFT. The frequency of simulation data direct current is 8.76Hz and 17.52Hz. Such as Figure 4.9. At the same time, we can use the equation 2-40 to prove the frequency which is right. It is characteristic for the finite swing motion. We can determine the motion of the hammer by the

frequency.

When $\omega_A = 191.022$ rpm and $\omega_P = 286.533$ rpm , the locus of LED for the simulation is Figure 4.10. The locus of LED for the simulation is produced by the simulation software in 0.5 second. We put the top view of the planetary ball mill machine on the Figure 4.10. The biggest outer circle is the arm. The second largest circle is the top of the inside wall for the cup. The minimum circle is the down of the inside wall for the cup. Such as Figure 4.11. In Figure 4.11, we can find the louse of the LED for the hammer to touch the minimum circle. And, we can find the louse of the LED for the hammer to run the leave half of the cup. It is characteristic for the finite swing motion. We can determine the motion of the hammer by the characteristic of the louse for the hammer.

So, When $\omega_A = 191.022$ rpm and $\omega_P = 286.533$ rpm, we can use two method to determine the specific of the motion for the hammer which is in the cup. One method is the frequency of the direct current for the motor. Another method is the locus of LED for the hammer from the photo picture. If the experimental data conform to the simulation data, we can determine the finite swing motion of the hammer which is in the cup. At same time, we can find the normal force, the friction force, ω and ω_H .

4.1.2 Continuous rotation motion

When $\omega_A = 71.633$ rpm and $\omega_P = 573.066$ rpm, the motion the hammer is the continuous rotation motion. The number of θ is accumulating. Such as Figure 4.12. The motion is the hammer which mill

between 0°～-360°on inboard wall of the cup. Such as Figure 4.13. The number of the normal force is among 31N～48N. Such as Figure 4.14. The number of normal force of the hammer can change the size of the powder. If the normal force of the hammer is bigger, the size of the powder is smaller . The number of the friction force is among 4.6N～7.2N. Such as Figure 4.15. The number of the friction force have relations with the number of the normal force. When the number of the normal force is greater, the number of the friction is greater, too. According to the equation 2-51 and the equation 2-52, we can find the torque to have relation with the friction. And, according to the equation 2-55 and the equation 2-56, we can find the direct current of the power to have relation with the torque. So, when the friction force is greater, the change of the direct current for the power is greater. ω is among 50rad/s～-53.8rad/s. Such as Figure 4.16. According to the equation 2-23. When ω is greater, the number of the normal force is greater, too. ω_H is among -84rad/s～-93.5rad/s rad/s. Such as Figure 4.17. According to the equation 2-26. When ω_H is greater, the number of ω is greater, too. According to the equation 2.56. We can change from the torque to the current of power. K is coefficient of the motor B. So, the direct current of the power for the motor B is Figure 4.18. We must record 10000 data of direct current for the power every 10 ms. And, we can transform the direct current of the power into the frequency with FFT. The frequency of simulation direct current is 14.33Hz. Such as Figure 4.19. It is characteristic for the continuous rotation motion. We can determine the motion of the hammer by the frequency.

When $\omega_A = 71.633$ rpm and $\omega_P = 573.066$ rpm, the locus of LED for the simulation is Figure 4.20. The locus of LED for the simulation is produced by the simulation software in 0.5 second. We put the top view of the planetary ball mill machine on the Figure 4.20. The biggest outer circle is the arm. The second largest circle is the top of the inside wall for the cup. The minimum circle is the down of the inside wall for the cup. Such as Figure 4.21. In Figure 4.21, we can find the louse of the LED for the hammer to be not touch the minimum circle. And, we can find the louse of the LED for the hammer to run the first half of the cup. It is characteristic for the continuous rotation motion. We can determine the motion of the hammer by the characteristic of the louse for the hammer.

So, When $\omega_A = 71.633$ rpm and $\omega_P = 573.066$ rpm, we can use two method to determine the specific of the motion for the hammer which is in the cup. One method is the frequency of the direct current for the motor. Another method is the locus of LED for the hammer from the photo picture. If the experimental data conform to the simulation data, we can determine the continuous rotation motion of the hammer which is in the cup. At same time, we can find the normal force, the friction force, ω and ω_H .

4.2 Experimental data

In the experiment, when the planetary ball mill machine runs, the direct current of power for the motor B is recorded. First, we measure the direct current with AD/DA card when the planetary ball mill machine runs

with no the hammer. Second, we measure the direct current with AD/DA card when the planetary ball mill machine runs with the hammer. And, the record need 10000 material. The record which is data of the direct current transforms into frequency with FFT. At the same time, we use a single-lens reflex camera to take the louse of LED which is set up the planetary ball mill machine.

In the experiment, we must control the angular velocity of the arm and the angular velocity of the cup. So, we must control the angular velocity of the motor A and the angular velocity of the motor B. According to the equation 3-7 and equation 3-8. The teeth of the planetary gear is fifty. The teeth of the sun gear is sixty-four. So, it is angular velocity of the cup.

$$\omega_P = -\frac{N_S}{N_P}\omega_S + \omega_A\left(\frac{N_S}{N_P} + 1\right) \tag{4.1}$$

And

$$r_r = 1 \tag{4.2}$$

According to the equation 4.1 and the equation 4.2. We can control the angular velocity of the motor A and the angular velocity of the motor B equably.

4.2.1 Finite swing motion

When $\omega_A = 191.022$ rpm and $\omega_P = 286.533$ rpm , the direct current of the power for the motor B is recorded. We must record 10000 data of direct current for the power every 10 ms. First, we measure the direct current of the power for the motor B when the planetary ball mill machine with no the hammer. Such as Figure 4.22. Second, we measure the

direct current of the power for the motor B when the planetary ball mill machine with the hammer. Such as Figure 4.23. In Figure 4.22 and Figure 4.23, we can find much noise. The noise is produced by the machine which can produce shake when the machine runs. The record which is with no the hammer is transforming into frequency with FFT. Such as Figure 4.24. The record which is with the hammer is transforming into frequency with FFT. Such as Figure 4.25. Especially, there are the low frequency in the Figure 4.24 and Figure 4.25. If the machine is assembled instability, the machine produces low frequency. So, the low frequency doesn't influence the direct current of the power for the motor B. And, we can use the Figure 4.24 to compare with Figure 4.25. We find difference in frequency between the Figure 4.24 and Figure 4.25. We must use the different frequency compare with simulation data and check the different frequency. If the different frequency conform to the simulation data, we can determine the specific of the motion of the hammer.

At the same time, we use a single-lens reflex camera to take the louse of the LED which is set up top of the hammer, the side of the arm and the side of the cup. Such as Figure 4.26. The locus of experiment is produce by the single-lens reflex camera in 0.5 second. We put the top view of the planetary ball mill machine on the Figure 4.26. The biggest outer circle is the arm. The second largest is the top of the inside wall for the cup. The minimum circle is the down of the inside wall for the cup. Such as Figure 4.27. In Figure 4.27, we can find the louse of the LED for the hammer to touch the minimum circle. And, we can find the louse of the LED for the hammer to run the leave half of the cup. So, we can determine the motion of the hammer is the finite swing motion form the louse of the experimental

data..

4.2.2 Continuous rotation motion

When $\omega_A = 71.633$ rpm and $\omega_P = 573.066$ rpm, the direct current of the power for the motor B is recorded. We must record 10000 data of direct current for the power every 10 ms. First, we measure the direct current of the power for the motor B when the planetary ball mill machine with no the hammer. Such as Figure 4.28. Second, we measure the direct current of the power for the motor B when the planetary ball mill machine with the hammer. Such as Figure 4.29. In Figure 4.28 and Figure 4.29, we can find much noise. The noise is produced by the machine which will produce shake when the machine run. The recorded which is with no the hammer is transforming into frequency with FFT. Such as Figure 4.30. The record which is with the hammer is transforming into frequency with FFT. Such as Figure 4.31. Especially, there are the low frequency in the Figure 4.30 and Figure 4.31. If the machine is assembled instability, the machine produces low frequency. So, the low frequency doesn't influence the direct current of the power for the motor B. And, we can use the Figure 4.30 to compare with Figure 4.31. We find difference in frequency between the Figure 4.30 and Figure 4.31. We must use the different frequency compare with simulation data and check the different frequency. If the different frequency conform to the simulation data, we can determine the specific of the motion of the hammer.

At the same time, we use a single-lens reflex camera to take the louse of LED which is set up top of the hammer、the side of the arm and the side

of the cup. Such as Figure 4.32. The locus of experiment is produce by the single-lens reflex camera in 0.5 second. We put the top view of the planetary ball mill machine on the Figure 4.32. The biggest outer circle is the arm. The second largest circle is the top of the inside wall for the cup. The minimum circle is the down of the inside wall for the cup. Such as Figure 4.33. In Figure 4.33, we can find the louse of the LED for the hammer to be not touch the minimum circle. And, we can find the louse of the LED for the hammer to run the first half of the cup. So, we can determine the motion of the hammer is the continuous rotation motion form the louse of the experimental data.

4.3 Data compares from the simulation analysis and the experimental data

In $\omega_A = 191.022$ rpm and $\omega_P = 286.533$ rpm , the motion of the hammer is the finite swing motion in simulation. The frequency of the simulation direct current is Figure 4.9. The frequency of the experimental direct current is Figure 4.24. We use the Figure 4.9 compare with Figure 4.24. We can find the same frequency which is 8.76Hz and 17.52Hz in the Figure 4.9 and the Figure 4.24. In addition, the simulation louse of the LED for the planetary ball mill machine is Figure 4.10. The experimental louse of the LED for the planetary ball mill machine is Figure 4.26. We use Figure 4.10 compare with Figure 4.26 at the same time. We can find the same louse in the Figure 4.10 and the Figure 4.26. So the frequency of the experimental data conform with the frequency of the simulation data and the louse of the experimental data conform with the louse of the simulation

data. So, When $\omega_A = 191.022$ rpm and $\omega_P = 286.533$ rpm , we can determine the motion of the hammer is the finite swing motion. And we can determine the normal of the hammer, the friction of the hammer, ω and ω_H form simulation data.

In $\omega_A = 71.633$ rpm and $\omega_P = 573.066$ rpm, the motion of the hammer is the continuous rotation motion in simulation. The frequency of the simulation direct current is Figure 4.30. The frequency of experimental direct current is Figure 4.28. We use Figure 4.19 to compare with Figure 4.30. We can find the same frequency which is 14.33Hz. In addition, the simulation louse of the planetary ball mill machine is Figure 4.20. The experimental louse of the planetary ball mill machine is Figure 4.32. We use Figure 4.20 compare with Figure 4.32 at the same time. We can find the same louse in Figure 4.20 and Figure 4.32. So the frequency of the experimental data conform with the frequency of the simulation data and the louse of the experimental data conform with the louse of the simulation data. So, When $\omega_A = 71.633$ rpm and $\omega_P = 573.066$ rpm, we can determine the motion of the hammer is the continuous rotation motion. And we can determine the normal of the hammer, the friction force of the hammer, ω and ω_H form simulation data.

We can know the effect of the planetary ball mill machine when the planetary ball mill machine run. But. in order to reach the best result when the planetary ball mill machine run, the data of the experiment compare with the data of the simulation. And, we know the best effect of the planetary ball mill machine when the motion of the hammer runs in the

continuous rotation motion. So, we must control the angular velocity of the arm and the angular velocity of the cup. As long as we can control the angular velocity of the arm and the angular velocity of the cup, we can control the planetary ball mill machine to reach the beat result.

Chapter 5 Conclusion

In the experiment, the finite swing motion and the continuous rotation motion had the effect of mill. But the continuous rotation motion had batter effect of mill. Because the normal force of the continuous rotation motion was batter big, and the range of the continuous rotation motion was batter many. The normal force could determine the size of the powder which is milled.

When the planetary ball mill machine run, the hammer would produce different motion by the coefficient of frictional force for the powder. So the motion of hammer was determined by the direct current of the power for the motor B which was transformed into frequency with FFT. If the motion of the hammer was the continuous rotation motion, the angular velocity of the arm could increase until the motion of the hammer was the finite swing motion. At the same time, the angular velocity of the arm could decrease a little until the motion of the hammer was the continuous rotation motion. It was the best effect of the planetary ball mill machine. If the motion of the hammer was the finite swing motion, the angular velocity of the arm and the s angular velocity of the cup could decrease until the motion of the hammer was the continuous rotation motion.

According to equation 2-23 and equation 2-24, we could find the change of the angular velocity for the arm and the change of the angular velocity for the cup to change the normal force. The change of t the angular velocity for the arm could be the square of the normal force. The change of the angular velocity for the cup could be multiple of the normal force. So, if the motion of the hammer was the finite swing motion in the beginning,

we should increase the angular velocity of the cup until the motion of the hammer was the continuous rotation motion. The angular velocity for the arm was decreased unless the angular velocity for the cup increased to limit.

So, the planetary ball mill machine should have the better effect. We should determine the motion of the hammer with the frequency of direct current for the motor B which was transformed with FFT. And, the frequency of the motion could determine with the simulation analysis. If the motion of the hammer was the continuous rotation motion in beginning, we should increase the angular velocity of the cup until a limit. The motion of the hammer was the continuous rotation motion all the same. Second step, we should increase the angular velocity of the arm until the motion of the hammer was the finite swing motion. At the same time, the angular velocity of the arm could decrease a little until the motion of the hammer was the continuous rotation motion. At the moment, the effect of the planetary ball mill machine was better. If the motion of the hammer was the finite swing motion in beginning, we should increase the angular velocity of the cup until a limit. If the motion of the hammer was the continuous rotation motion, we should increase the angular velocity of the arm until the motion of the hammer was the finite swing motion. At the same time, the angular velocity of the arm could decrease a little until the motion of the hammer was the continuous rotation motion. But, we should increase the angular velocity of the cup until a limit and the motion of the hammer was finite swing motion. We should decrease the angular velocity of the arm until the motion of the hammer was the continuous rotation. At the moment, the effect of the planetary ball mill machine was better. So, we

could control the angular velocity of the arm and the angular velocity of the cup to determine the motion of the planetary ball mill machine

Reference

[1] Shu-Ping Huang, “Preparation and Characterizations of Photo-curable Montmorillonites-Epoxy Nanocomposites ”.碩士論文, 國立交通大學, 2005

[2] Huang, Chia-Lin, “Modeling and Application of Planetary Gear Train ”. 碩士論文, 國立中山大學, 1993

[3] Chih-Hao Ma, “The Study of Nanolization of Slag” , 碩士論文, 國立中興大學, 2004

[4] Chun-Chieh Liang, “Dynamic Load Analysis of Planetary Gear System”, 碩士論文, 中華大學, 2005

[5] CHEN, GUANG-YU, “以行星式研磨方式進行光學元件製作之探討”, 碩士論文, 輔仁大學, 1981

[6] Chih-Hao Ma, “The Study of Nanolization of Slag”, 碩士論文, 國立中興大學, 2004

[7] Abdellaoui, M.; Gaffet, E., “Physics of mechanical alloying in the planetary ball mill and the horizontal hammer mill: kinematic approach”, Materials Science Forum, Jun 27-Jul 1 1994, p 339-344

[8] dos Santos, Maria Aparecida P.; Costa, Celio A.,“Programa de Engenharia Metalurgica e de Materiais, COPPE/UFRJ, CEP 21945-970 Rio de Janeiro, RJ, Brazil”, Powder Technology, Oct 31 2006, p 84-88

[9] Chattopadhyay, P.P.; Manna, I.; Talapatra, S.; Pabi, S.K., “Mathematical analysis of milling mechanics in a planetary ball mill”, Materials Chemistry and Physics, 2001, p 85-94

Tables

Name	AC MOTOR	DC MOTOR	Remark
Factory	ADELLPOWER	YASKAWA	
Rated Output(W)	750	830	
Voltage	AC 220V	DIRECT CURRENT 48V	
Rated Torque(kg-cm)	36.6	32.4	
Rated Speed	3000	3000	
Weight(kg)	2.1	8.35	

Table 3.1 The specifications of the motor

Name	Specification	Remark
Computer(PC)	INTER CPU 2.0 WIN XP 120G Hard Disk	
Motion card(HAL-8506)	Six, configurable, axes position control for servos or stepper 9 encoder channels with a 32-bit counter 8 DAC channels with a 16-bit resolution PCI bus interface	
AD/DA card(HAL 8184)	8 A/D channels with 12-bit resolution 4 D/A channels with 16-bit resolution Full Isolated Analog I/O	

Table 3.2 The specifications of the control

Name	Code Name	Value	Remark(unit)
The coefficient of Dynamics friction force	μ_k	0.12	
The coefficient of Statics friction force	μ_s	0.3	
Inertia of rotation	J	0.5	
The radius of the arm	Ra	0.085	m
The coefficient of electric current	K	0.0055	
Mass of the cup	Mp	2.188	kg
Inertia of the mill cup	I_P	0.02	
Inertia of the arm	I_A	0.03	

Table 4.1 The parameter of the planetary ball mill machine

Figures

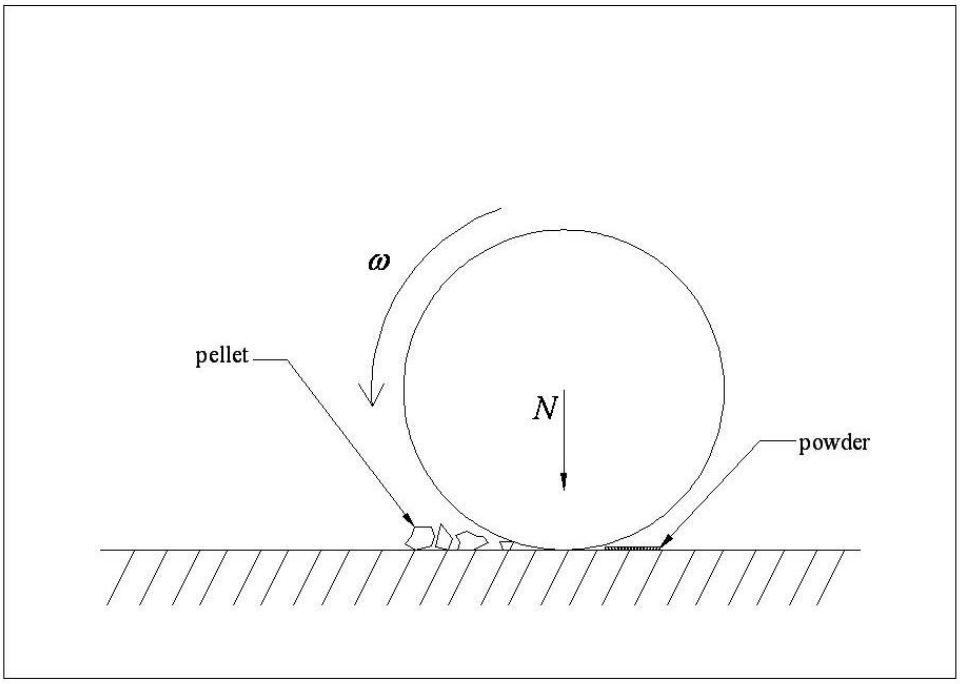

Figure 1.1 The wheel mills pellet to reach powder

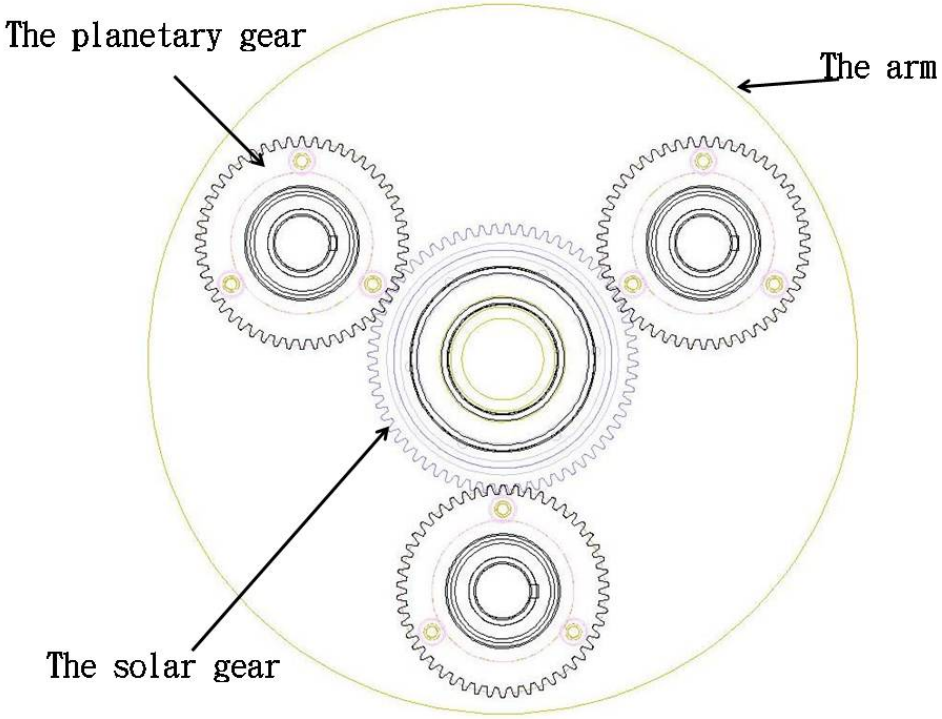

Figure 1.2 The upper side of direction for the planetary ball mill machine

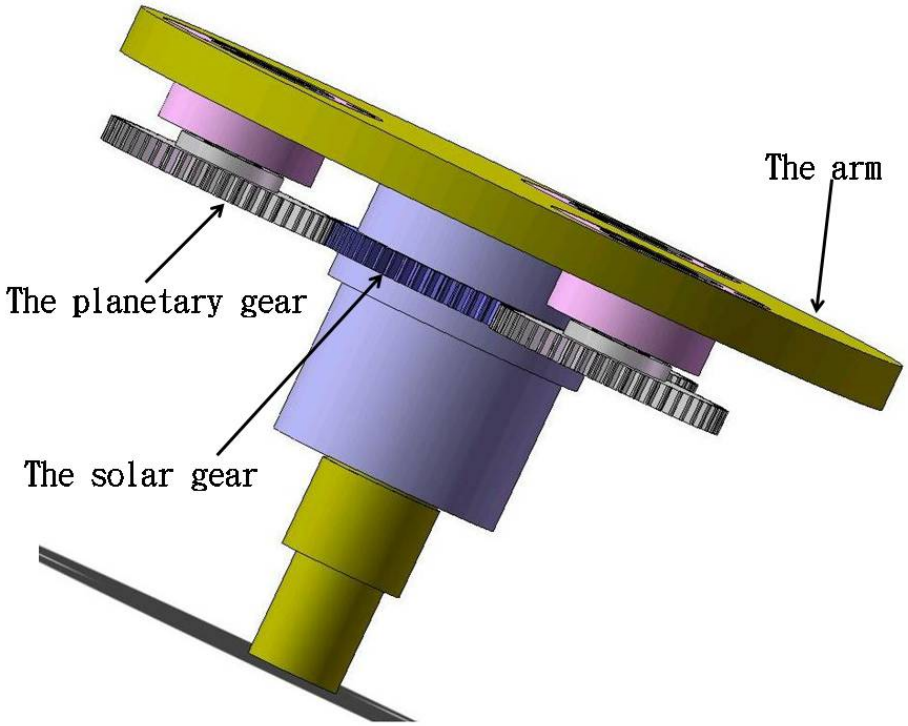

Figure 1.3 The assembly of the planetary ball mill machine

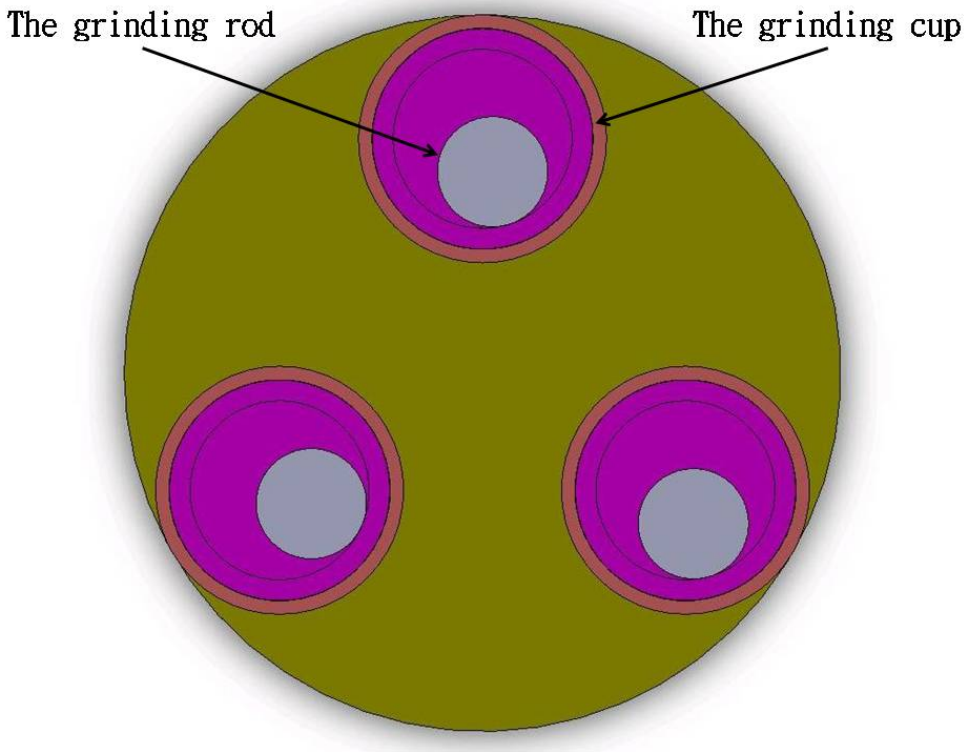

Figure 1.4 The assembly of the mill cup

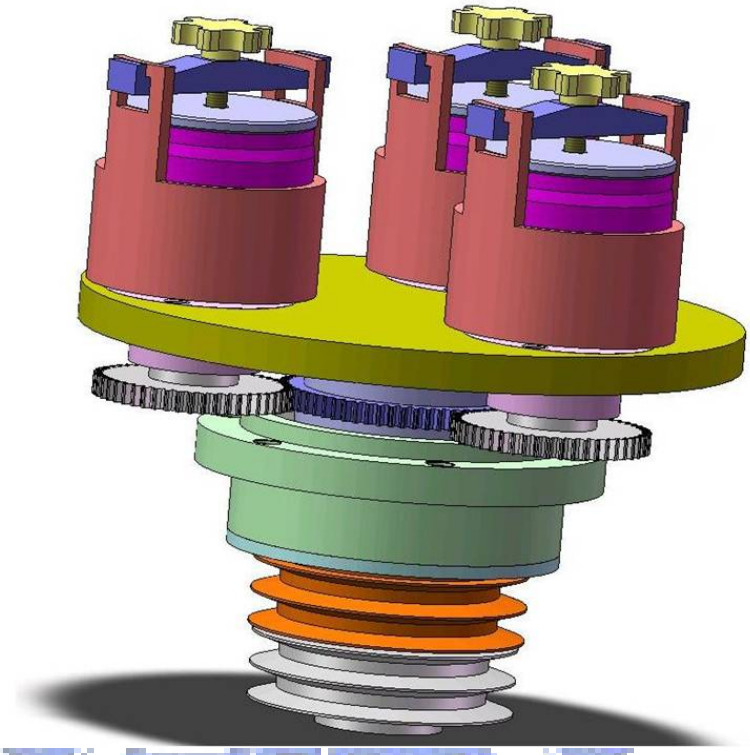

Figure 1.5The all assembly of the planetary ball mill machine

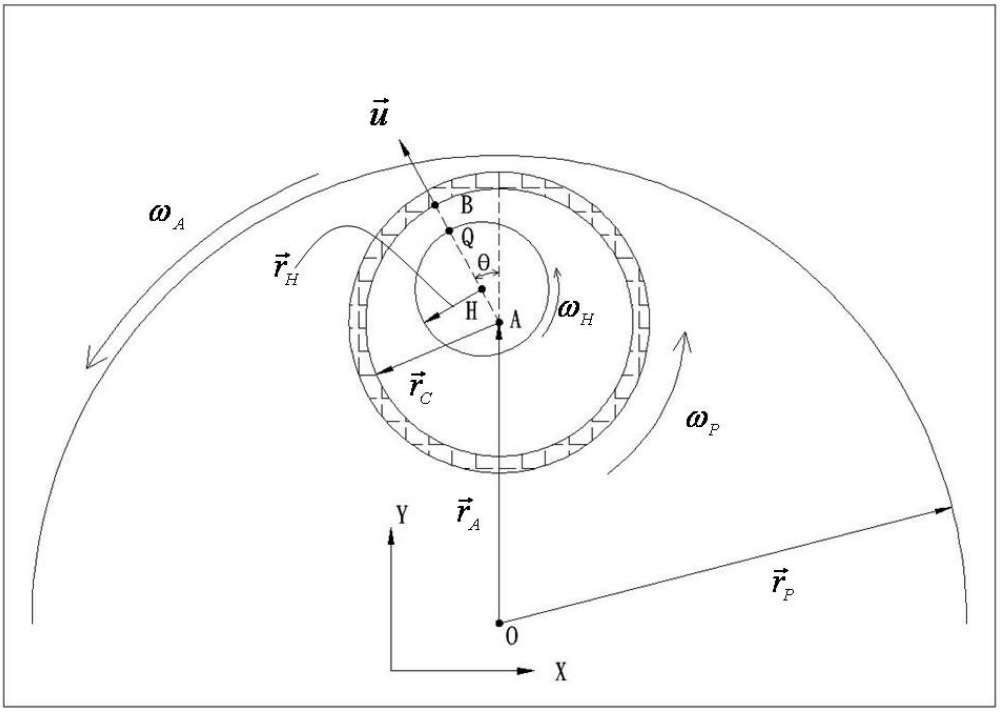

Figure 2.1 The motion of one mill cup and hammer

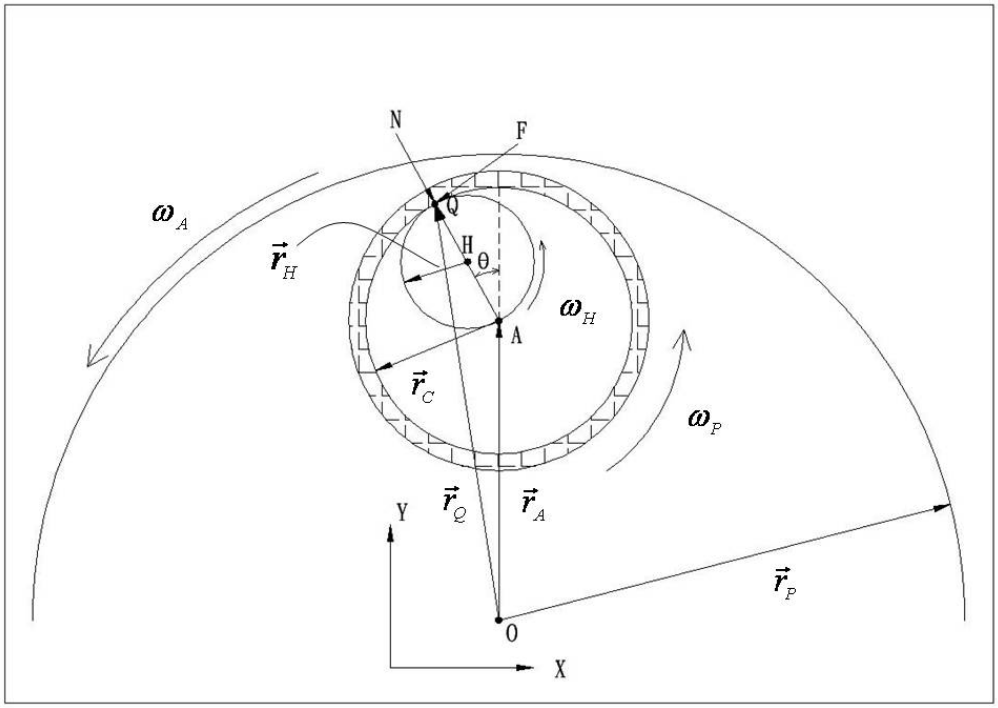

Figure 2.2 The contact motion

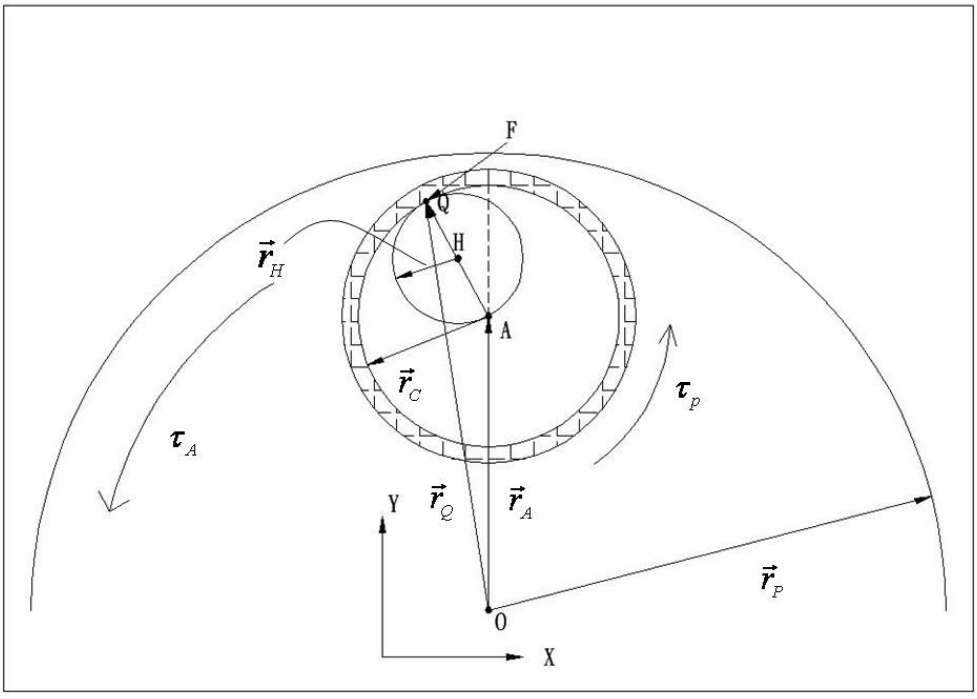

Figure 2.3 The layout of torque

Figure 3.1 The arm

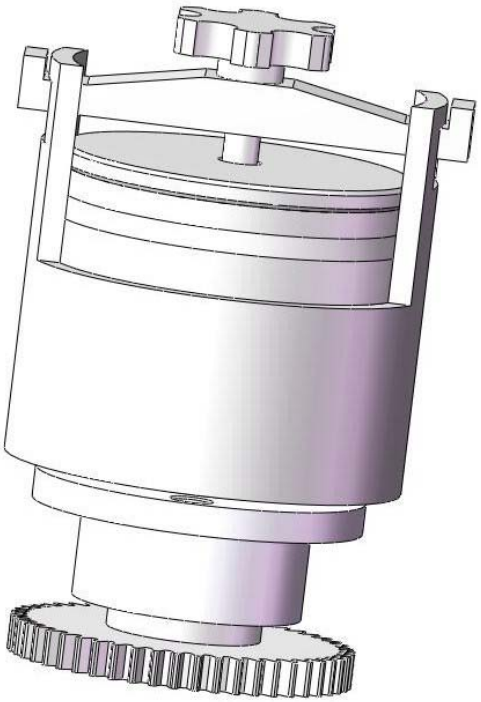

Figure 3.2 The cup

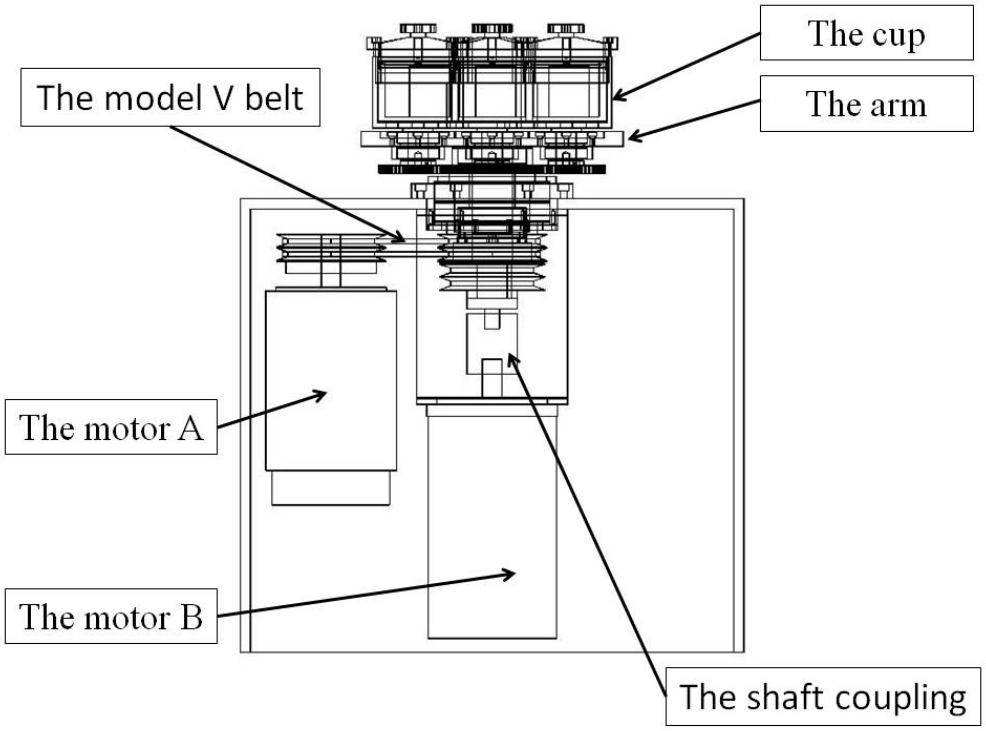

Figure 3.3 The layout of the motor A and the motor B

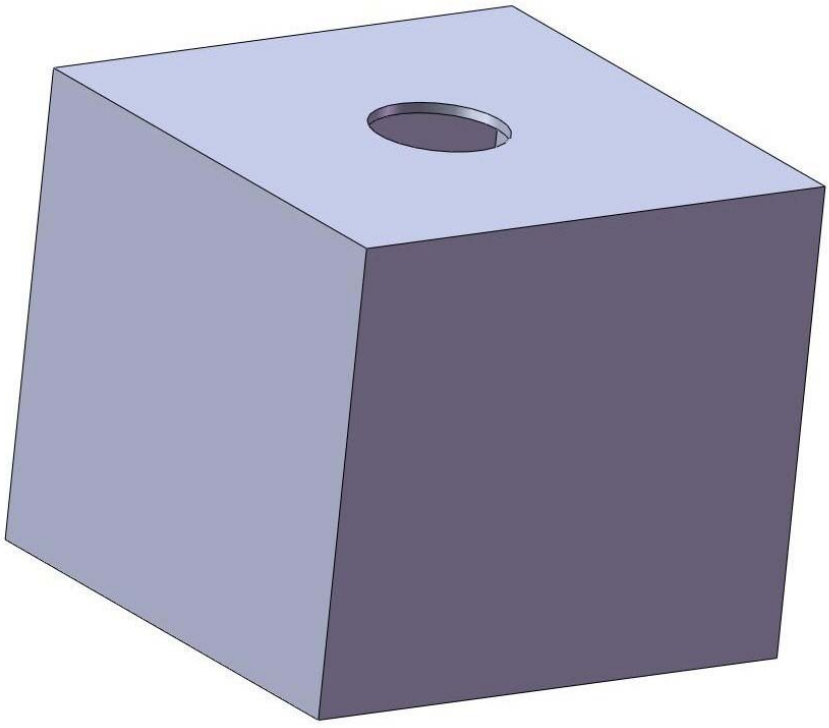

Figure 3.4 The framework

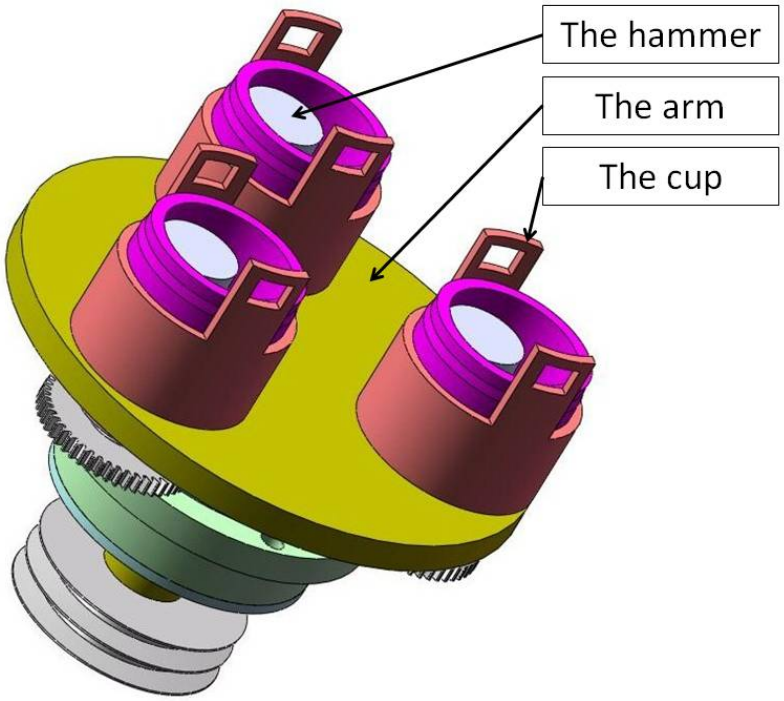

Figure 3.5 The planetary ball mill machine

Figure 3.6 The entity of the planetary ball mill machine

Figure 3.7 The hammer in the planetary ball mill machine

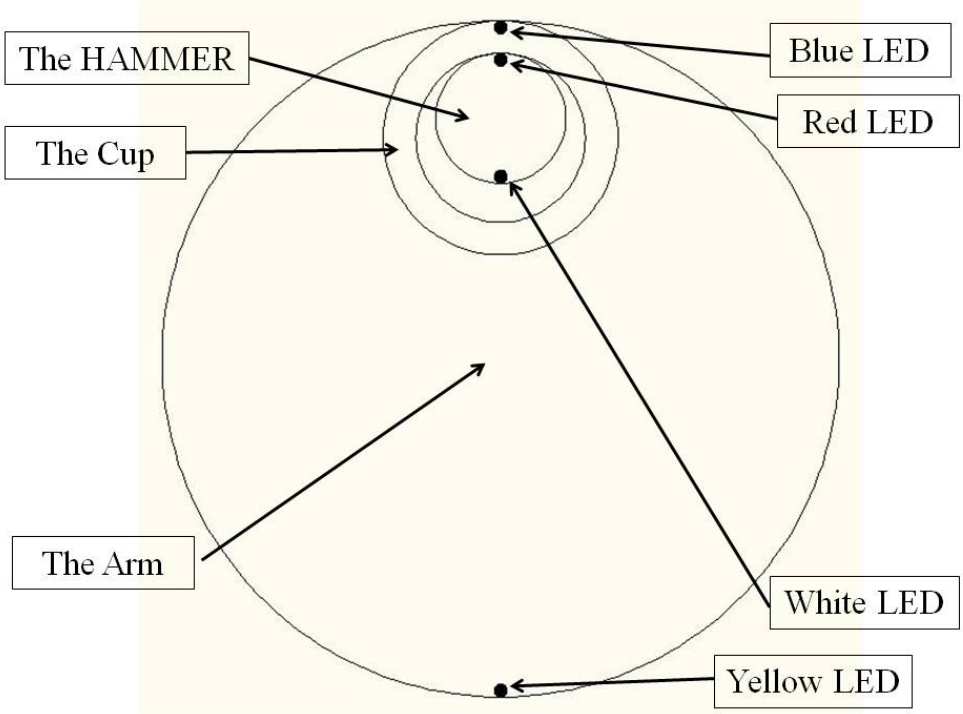

Figure 3.8 The layout of the LED which is set up the planetary ball mill machine

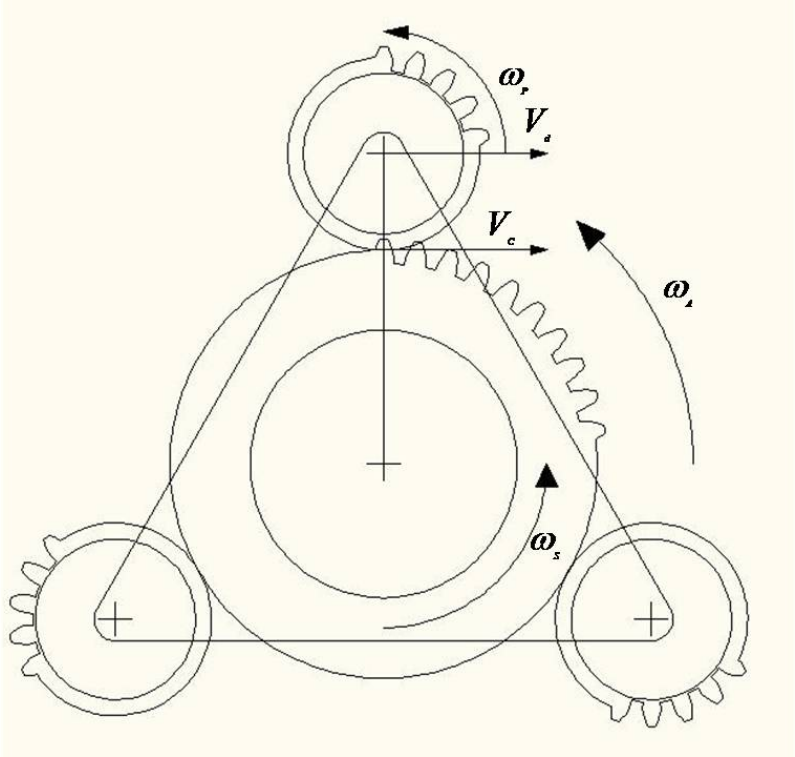

Figure 3.9 The angular velocity of the planetary gear

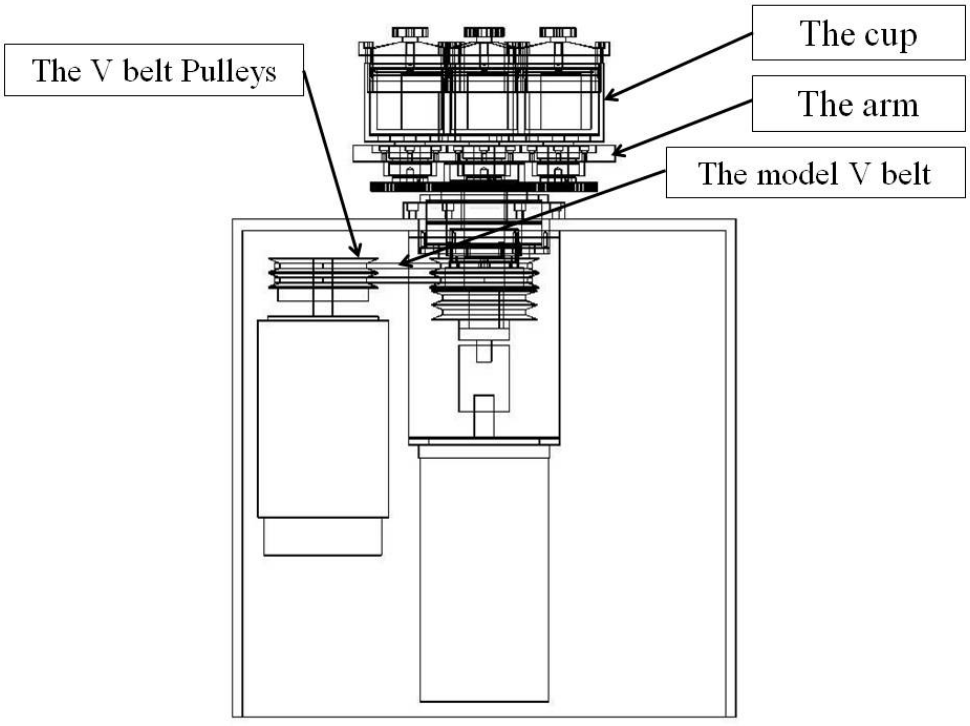

Figure 3.10 The model V belt and the model V belt pulleys

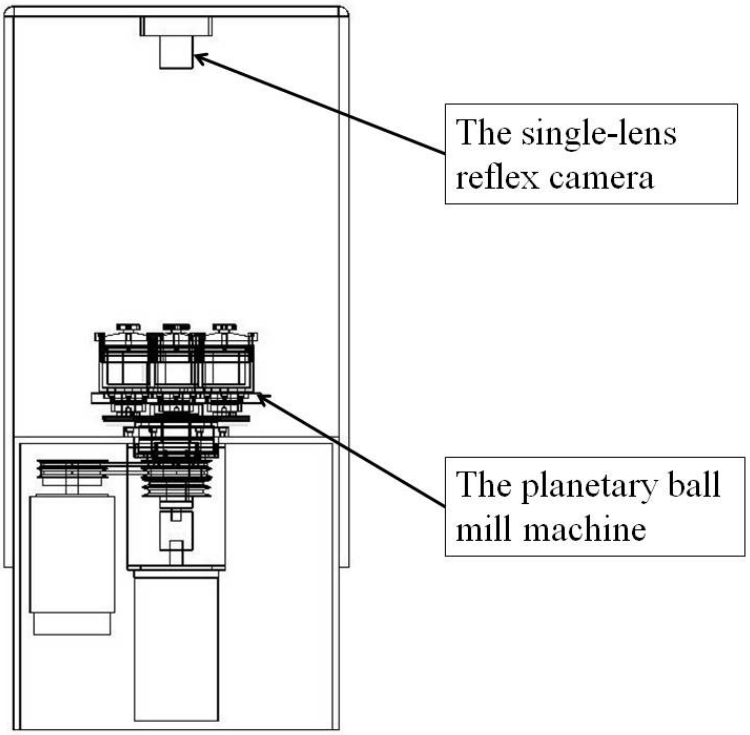

Figure 3.11 The single-lens reflex camera set up on top of the planetary ball mill machine

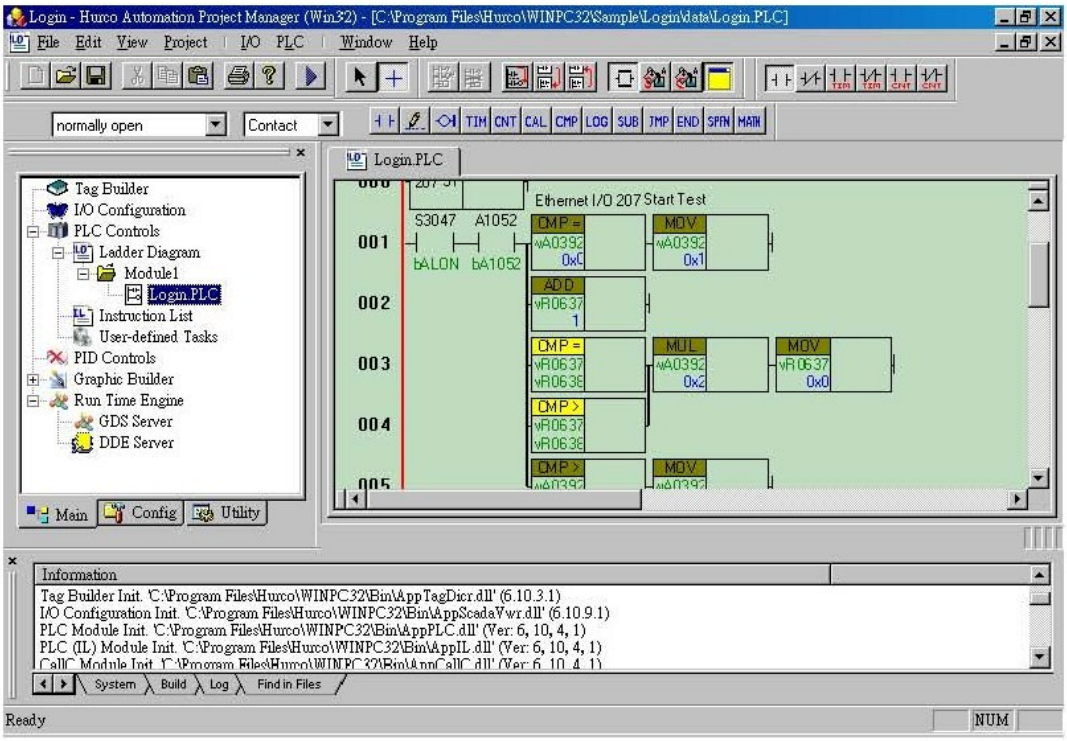

Figure 3.12 The WIN PC32

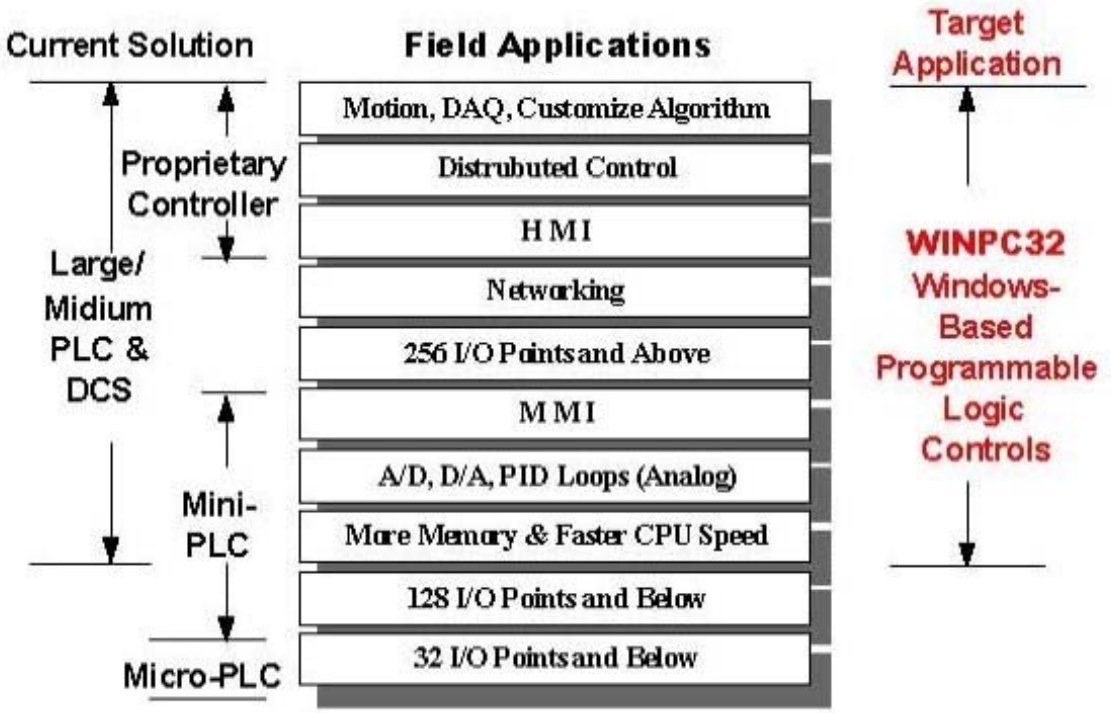

Figure 3.13 The Range of application for WIN PC32

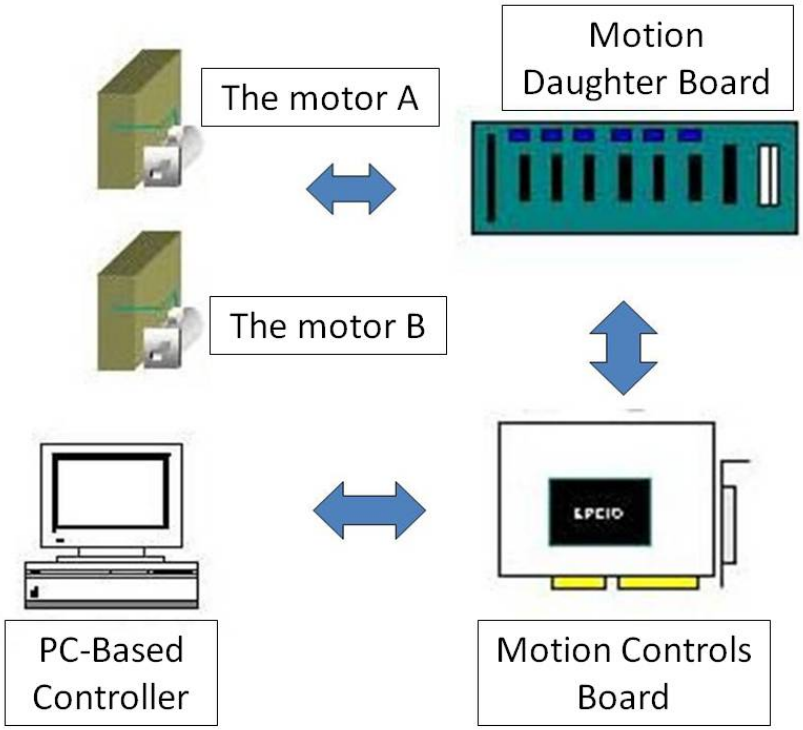

Figure 3.14 The control plane

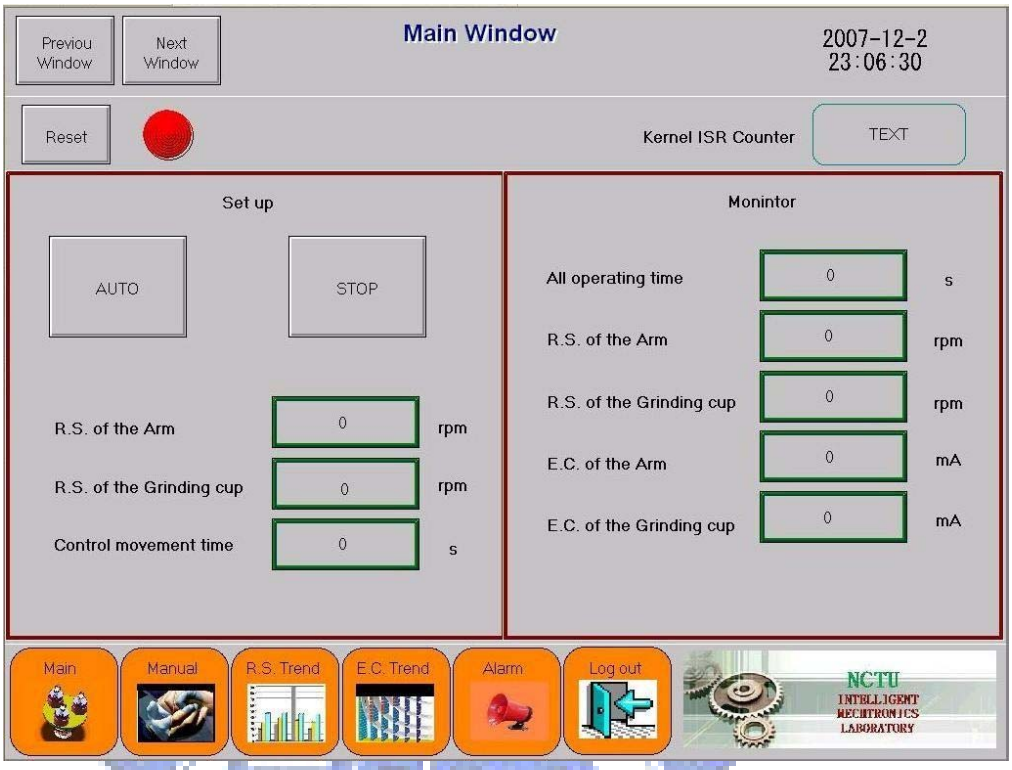

Figure 3.15 The main interface of the HMI

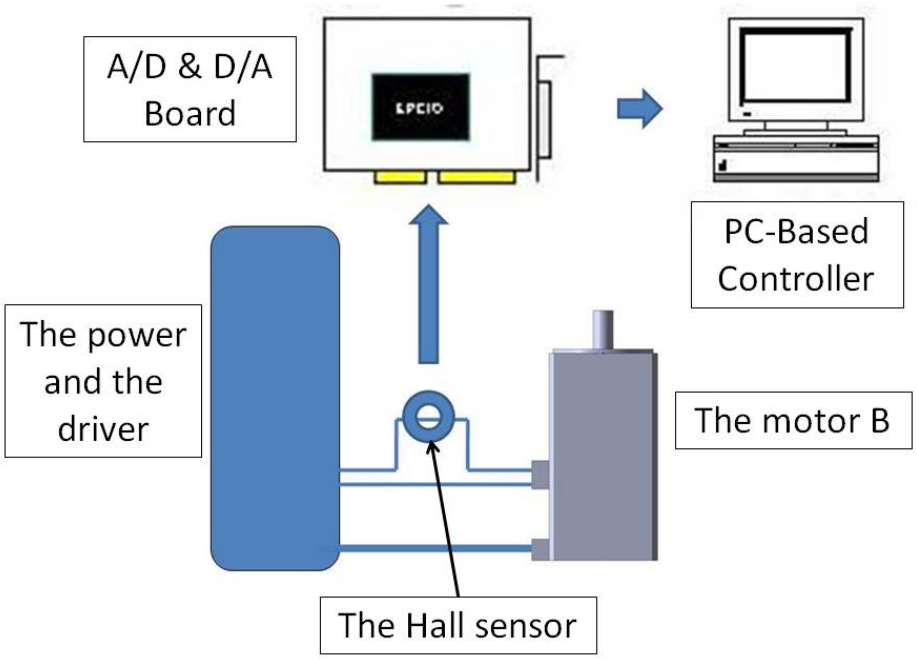

Figure 3.16 The AD/DA card and the hall sensor

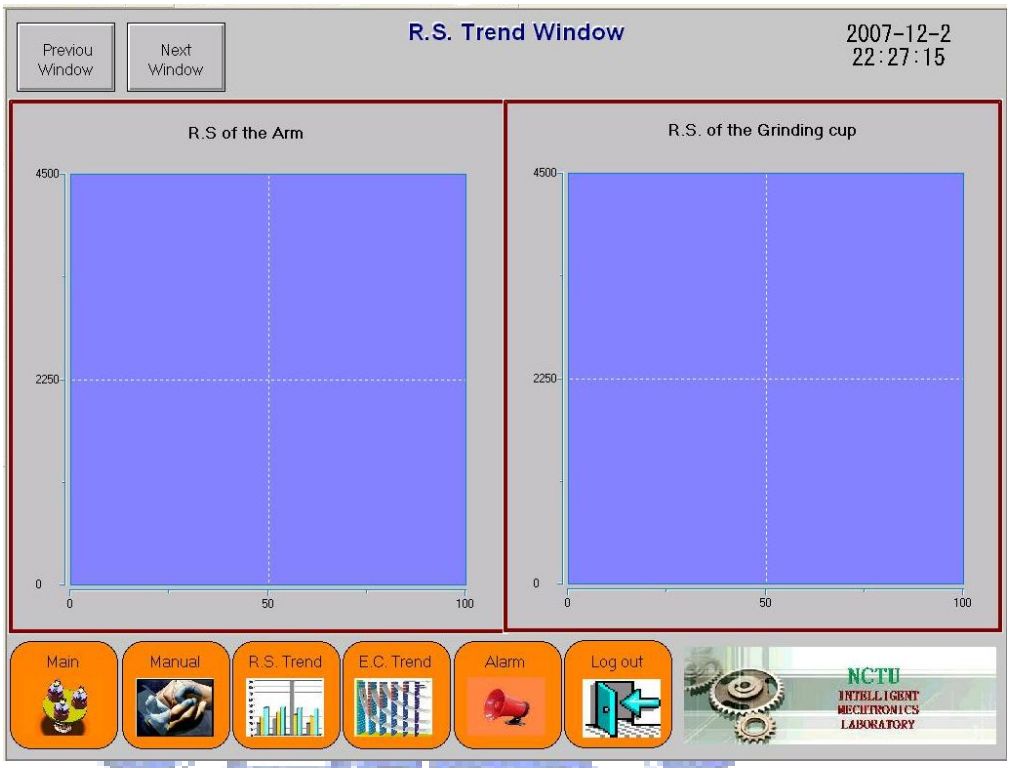

Figure 3.17 The R.S. Trend window of the HMI

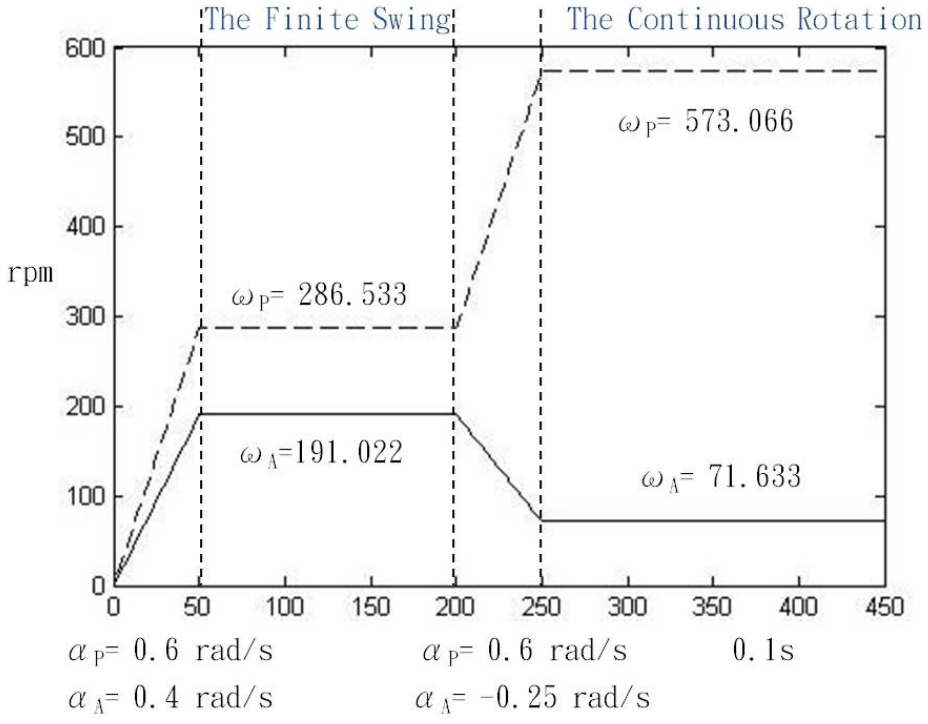

Figure 4.1 The layout of the angular velocity

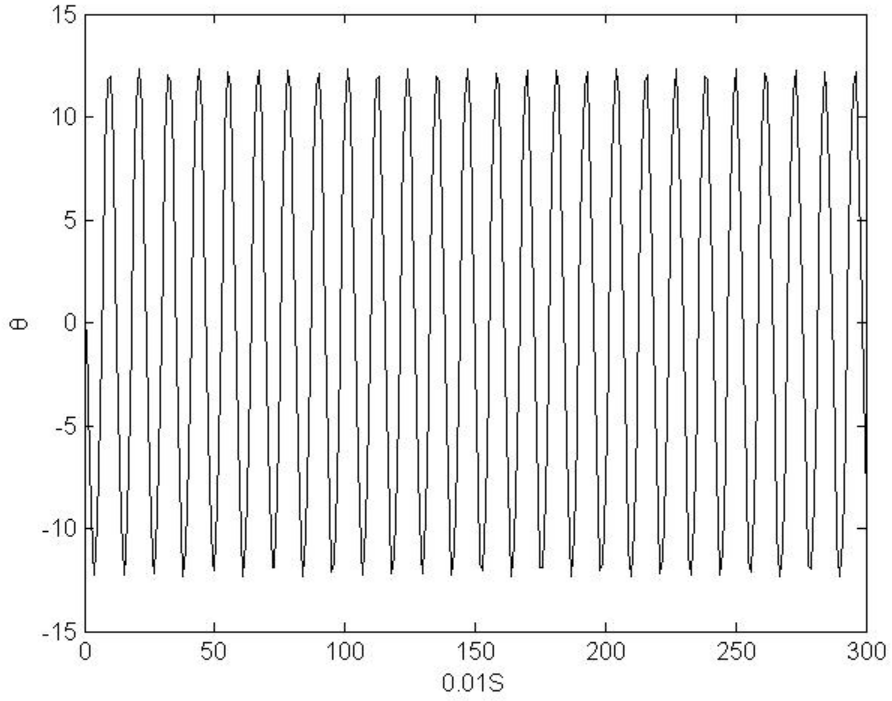

Figure 4.2 The θ of the finite swing motion form simulation

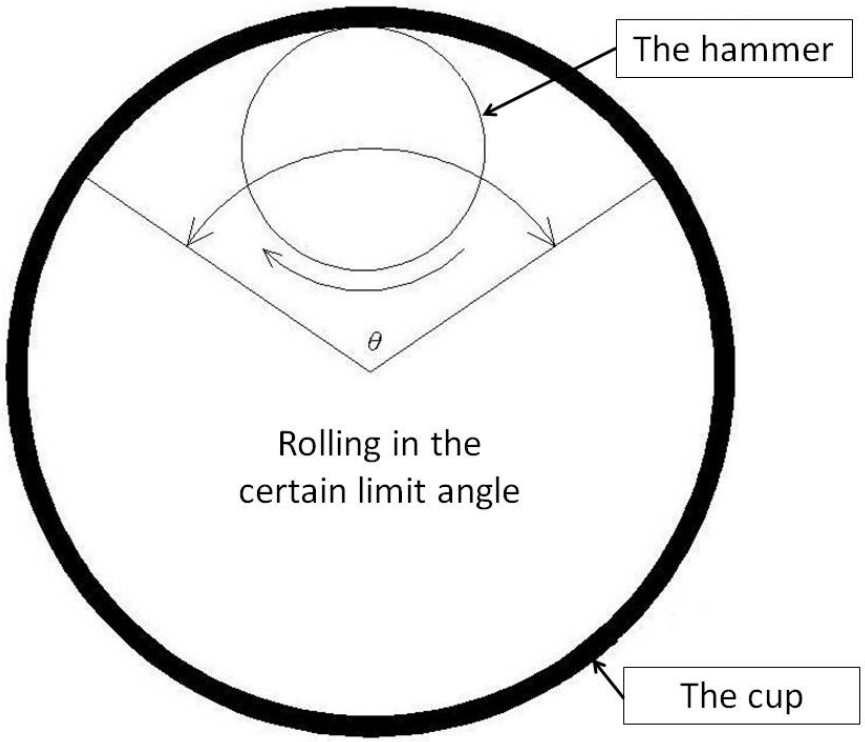

Figure 4.3 The finite swing motion form simulation

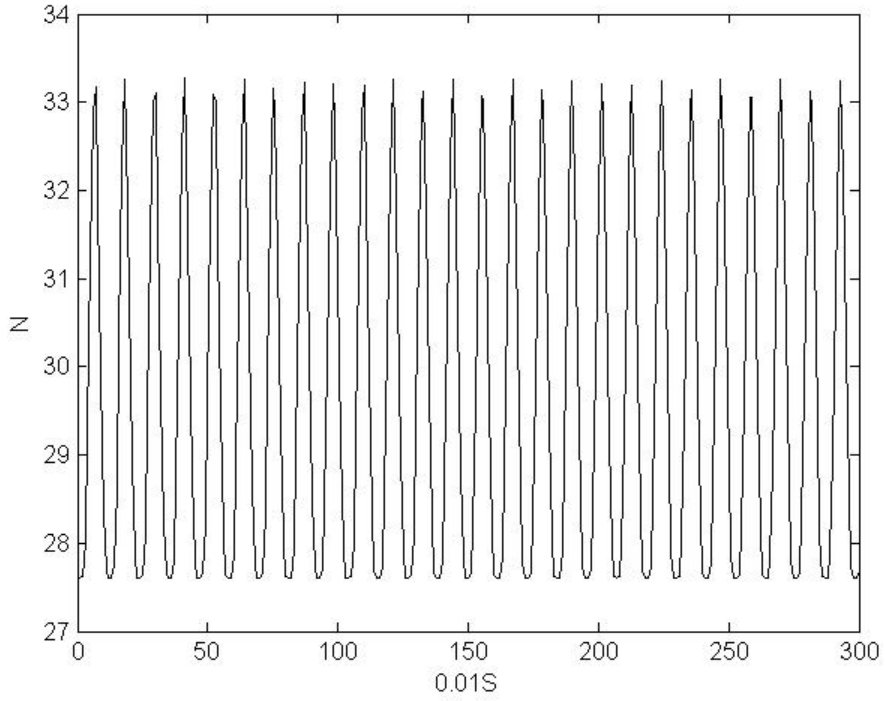

Figure 4.4 The normal force of the finite swing motion form simulation

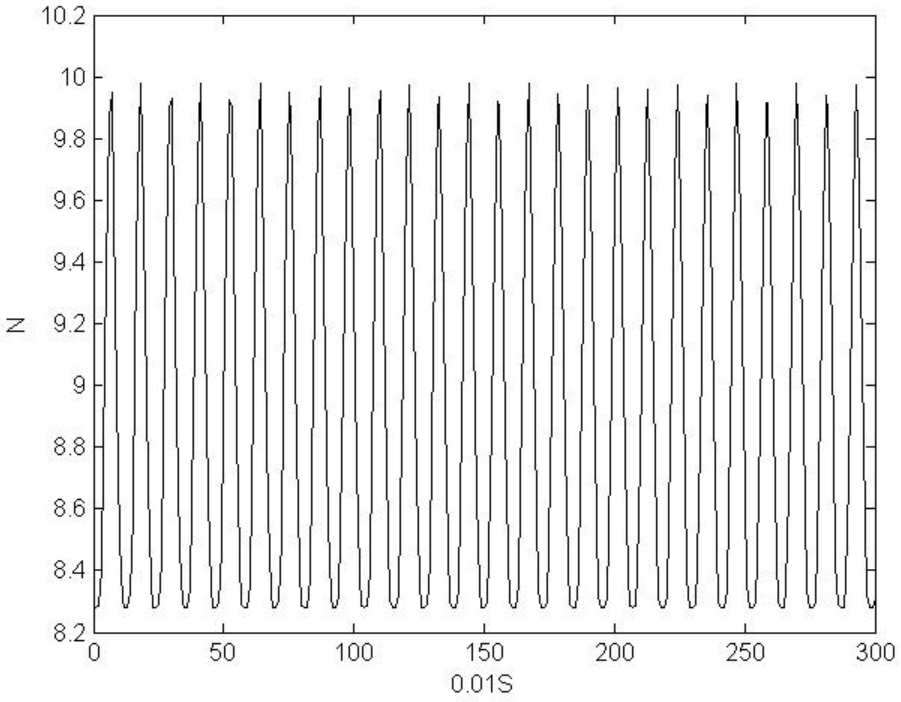

Figure 4.5 The friction force of finite swing motion form simulation

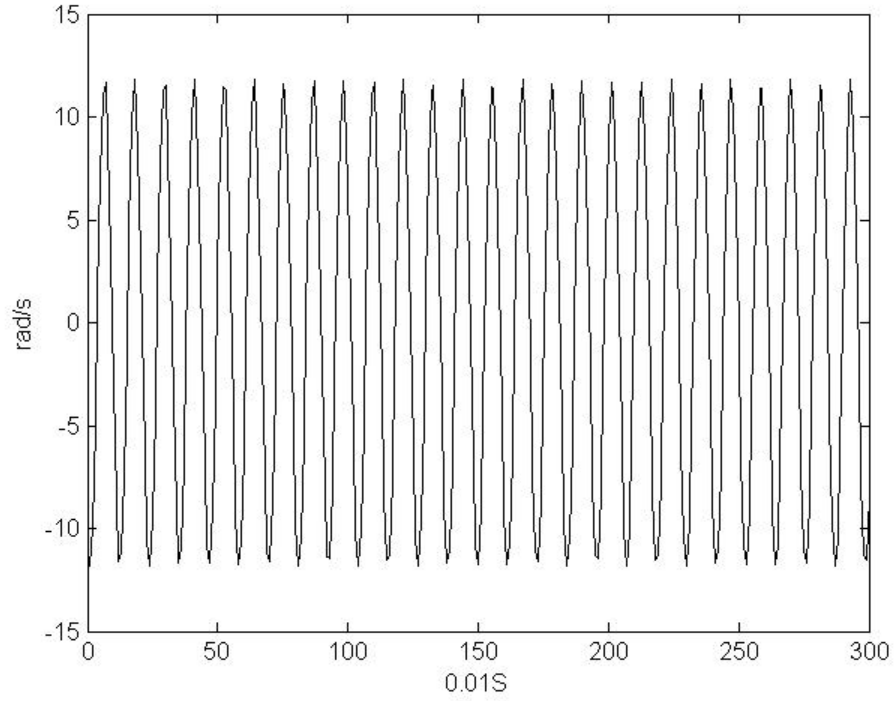

Figure 4.6 The ω of the finite swing motion form simulation

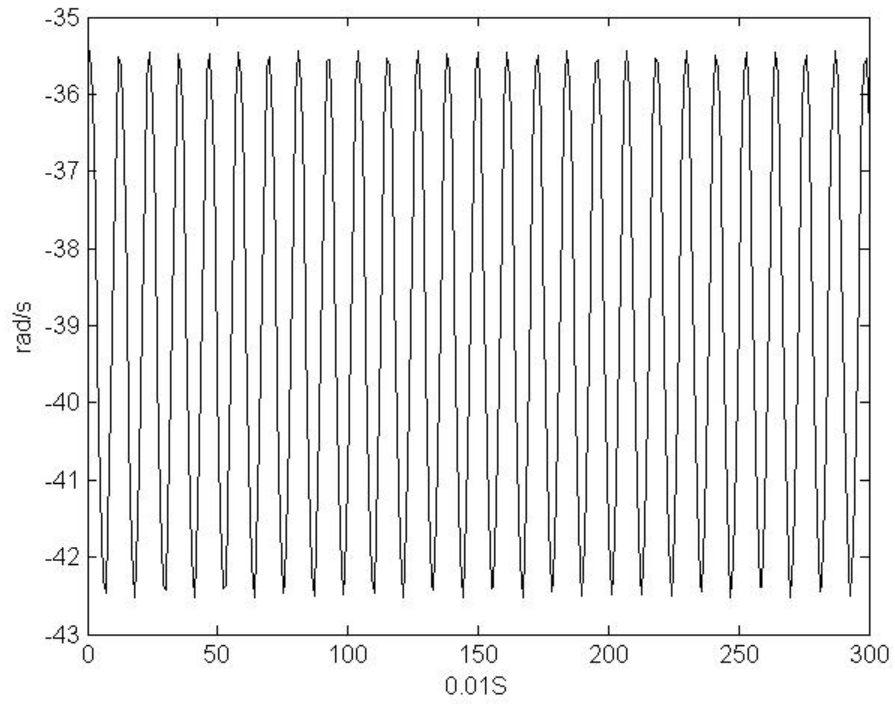

Figure 4.7 The ω_H of the finite swing motion form simulation

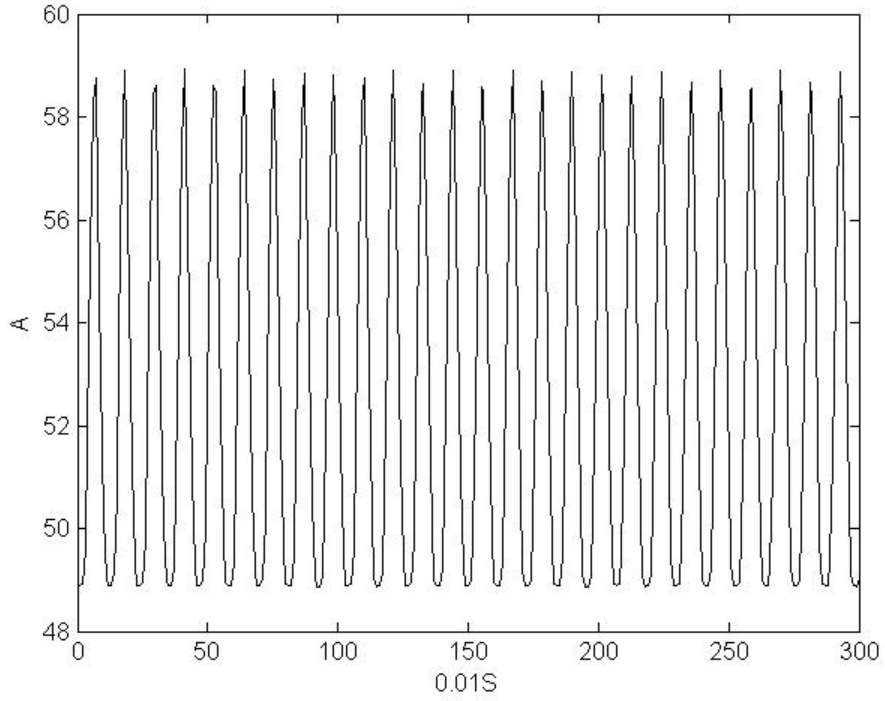

Figure 4.8 The direct current of finite swing motion form simulation

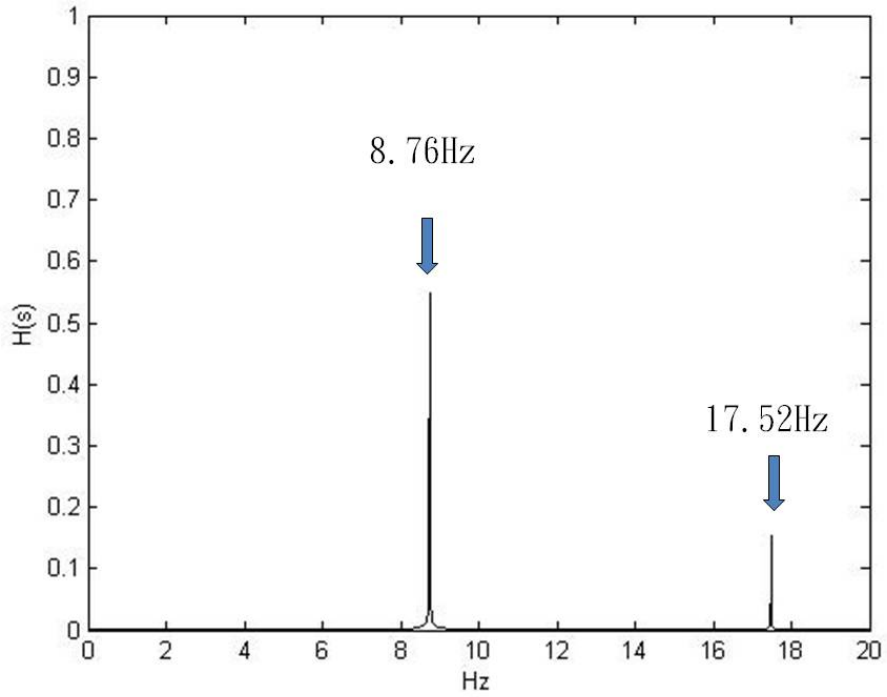

Figure 4.9 The FFT of the finite swing motion form simulation

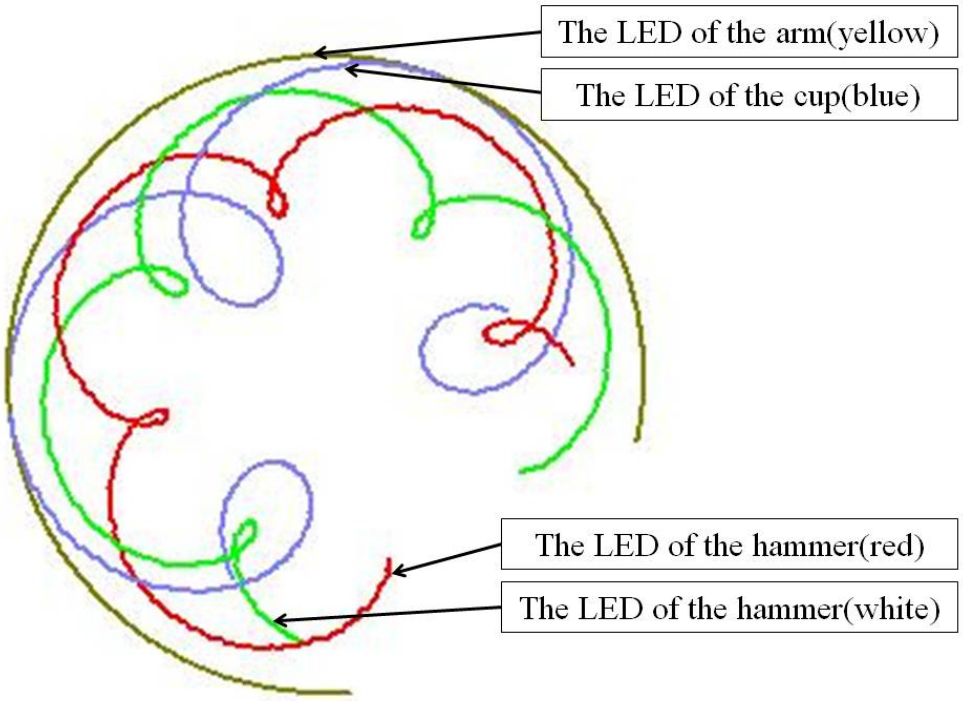

Figure 4.10 The louse of the finite swing motion form simulation

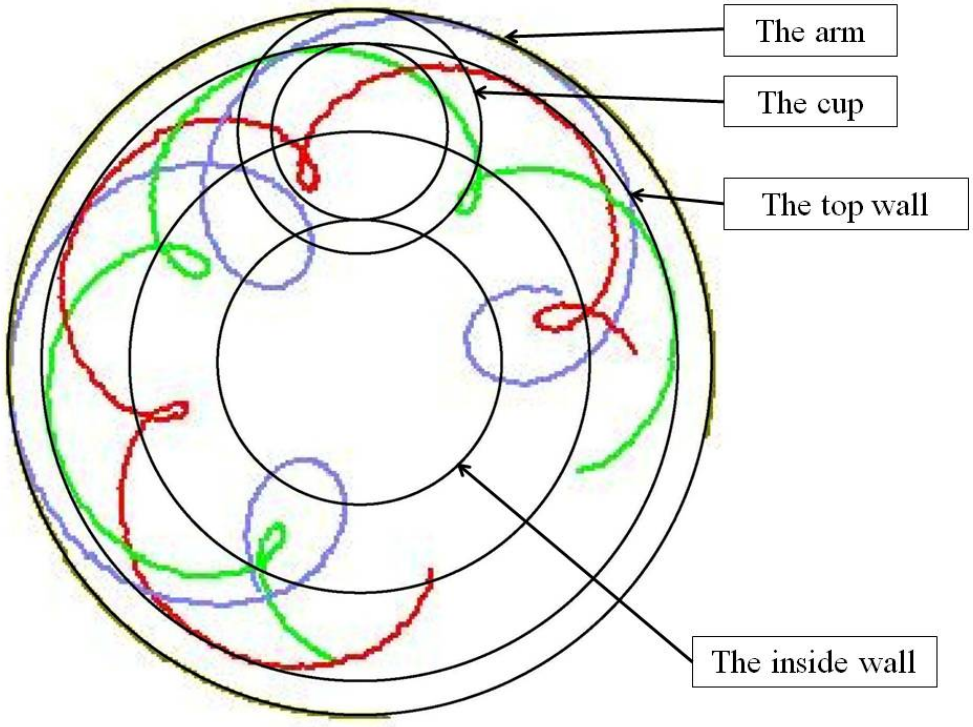

Figure 4.11 The top view on the louse of the finite swing motion form simulation

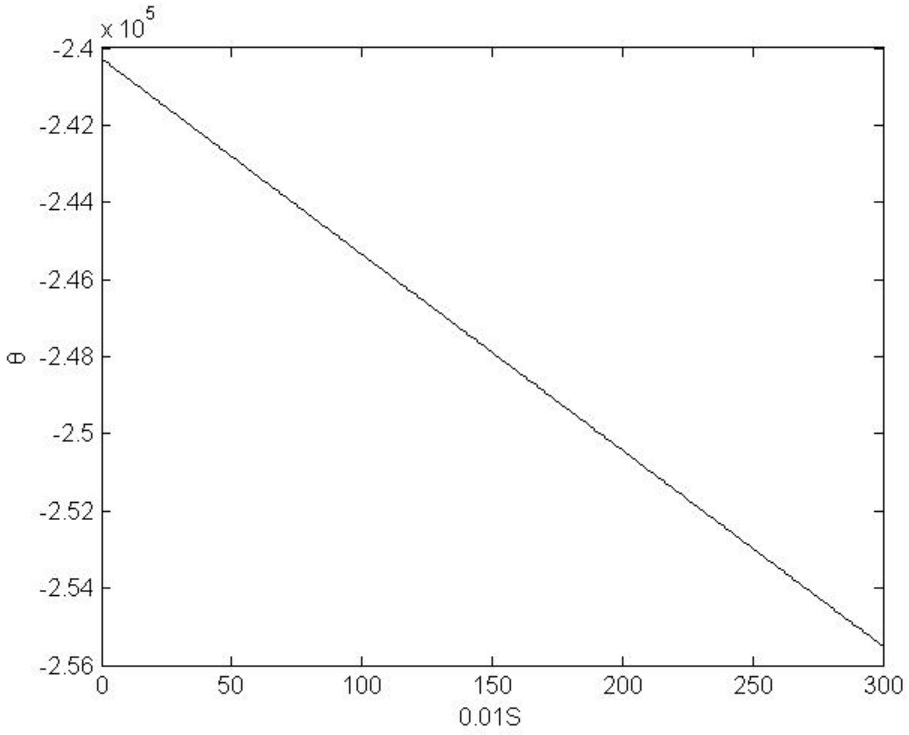

Figure 4.12 The θ of the continuous rotation motion form simulation

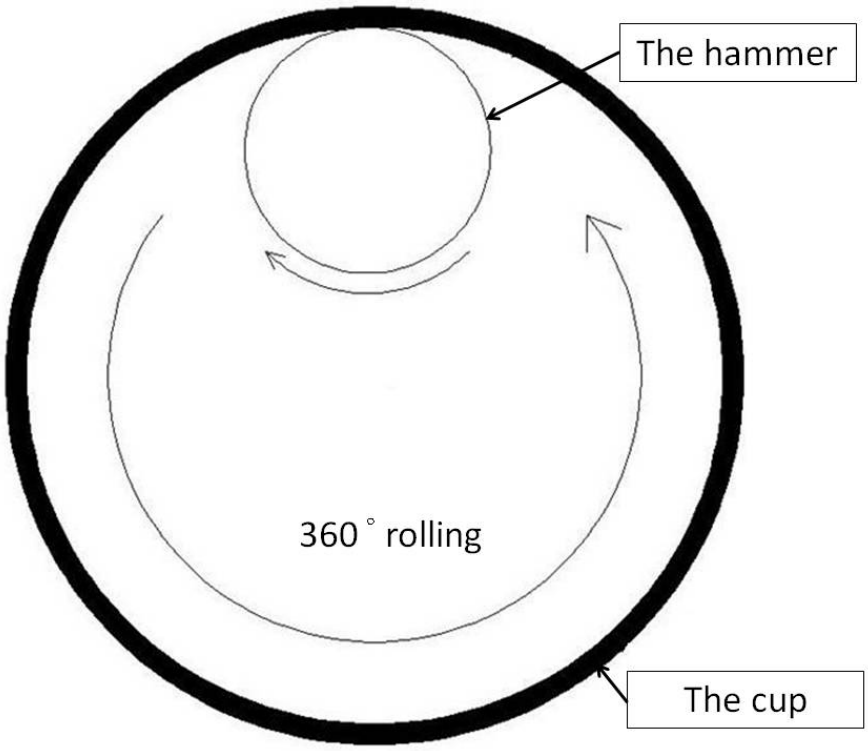

Figure 4.13 The continuous rotation motion form simulation

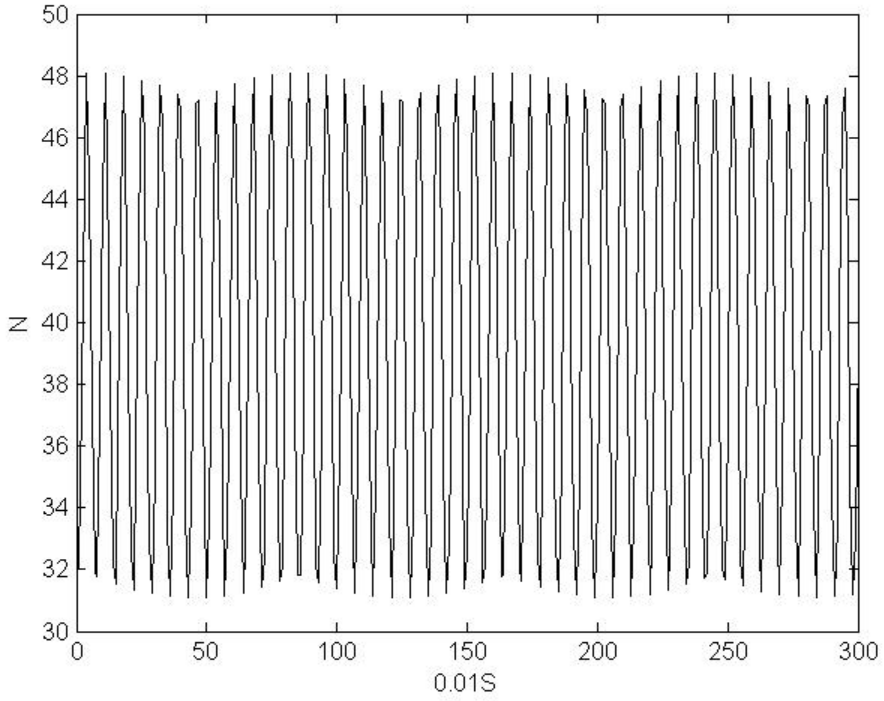

Figure 4.14 The normal force of the continuous rotation motion form simulation

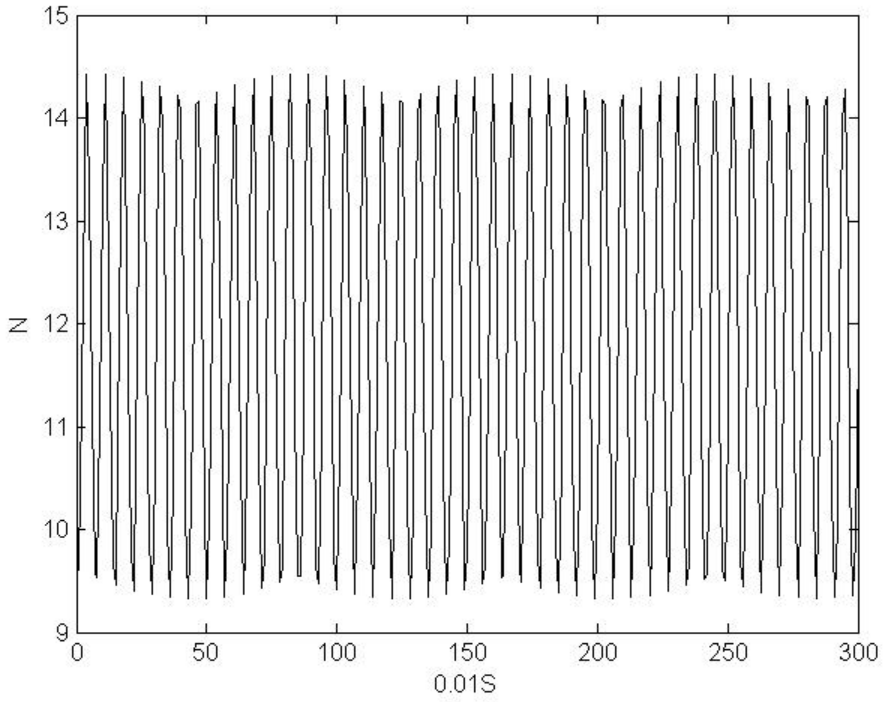

Figure 4.15 The friction force of the continuous rotation motion form simulation

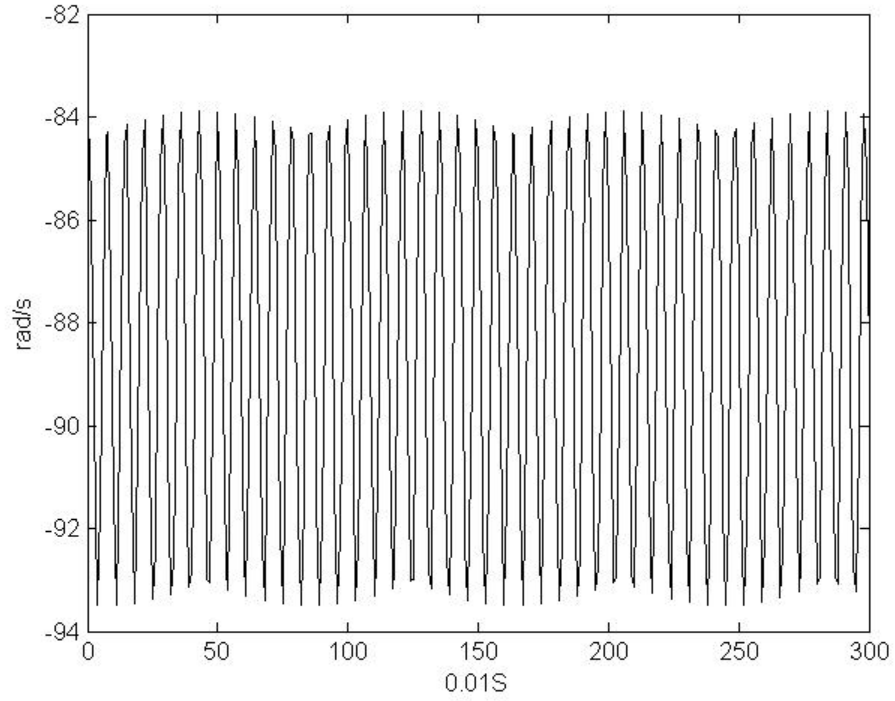

Figure 4.16 The ω of the continuous rotation motion form simulation

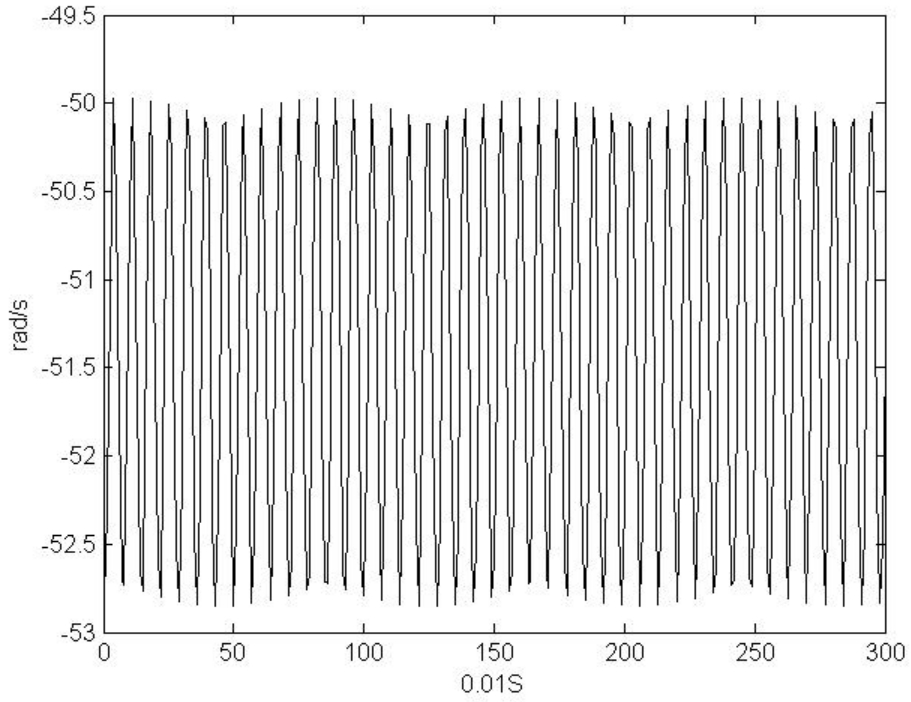

Figure 4.17 The ω_H of the continuous rotation motion form simulation

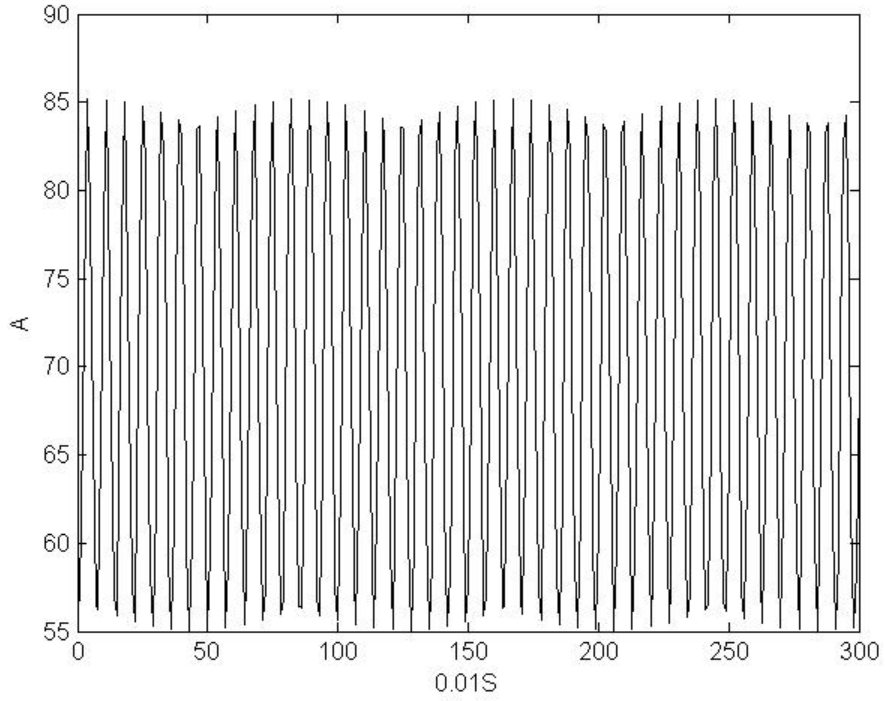

Figure 4.18 The direct current of the continuous rotation motion form simulation

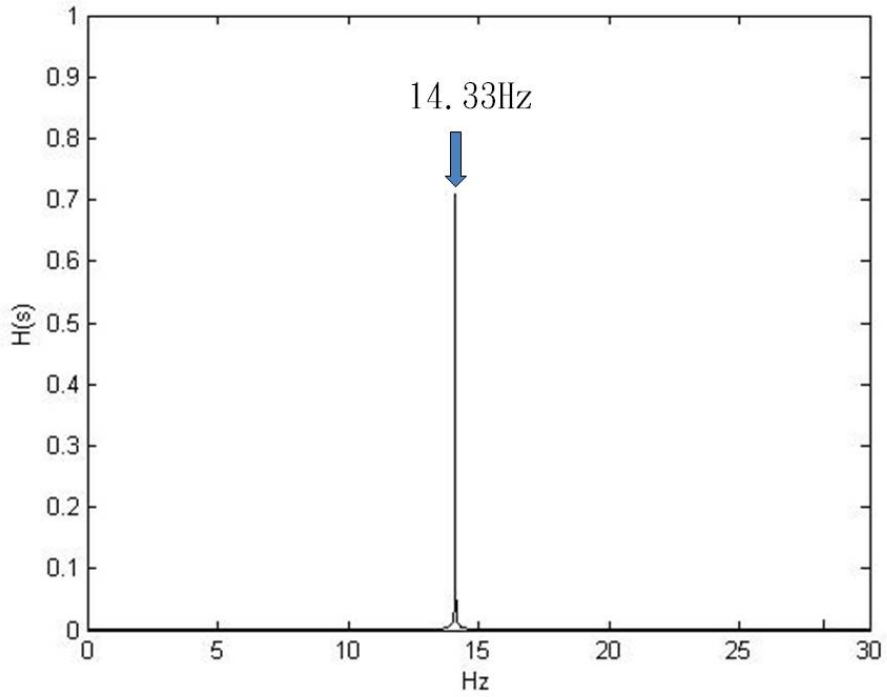

Figure 4.19 The FFT of the continuous rotation motion form simulation

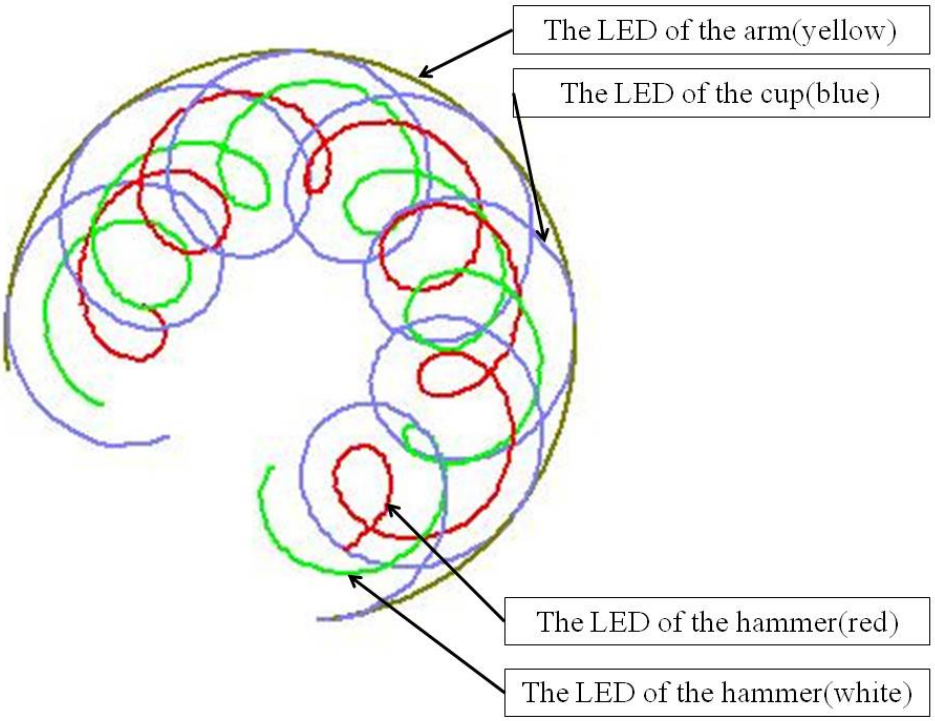

Figure 4.20 The louse of the continuous rotation motion form simulation

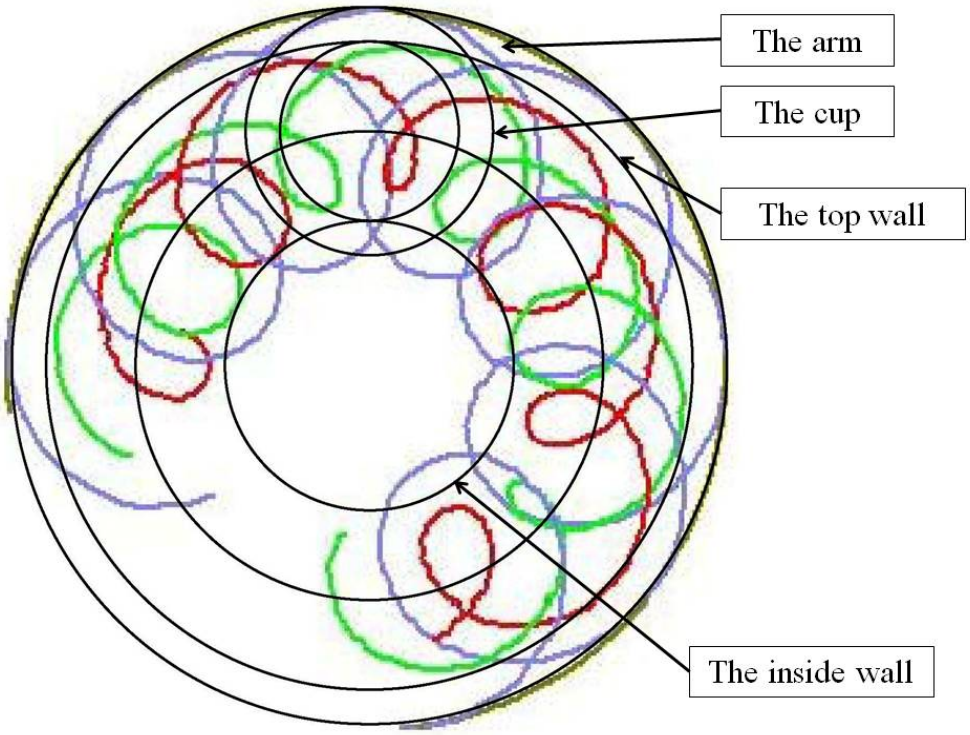

Figure 4.21 The top view on the louse of the continuous rotation motion form simulation

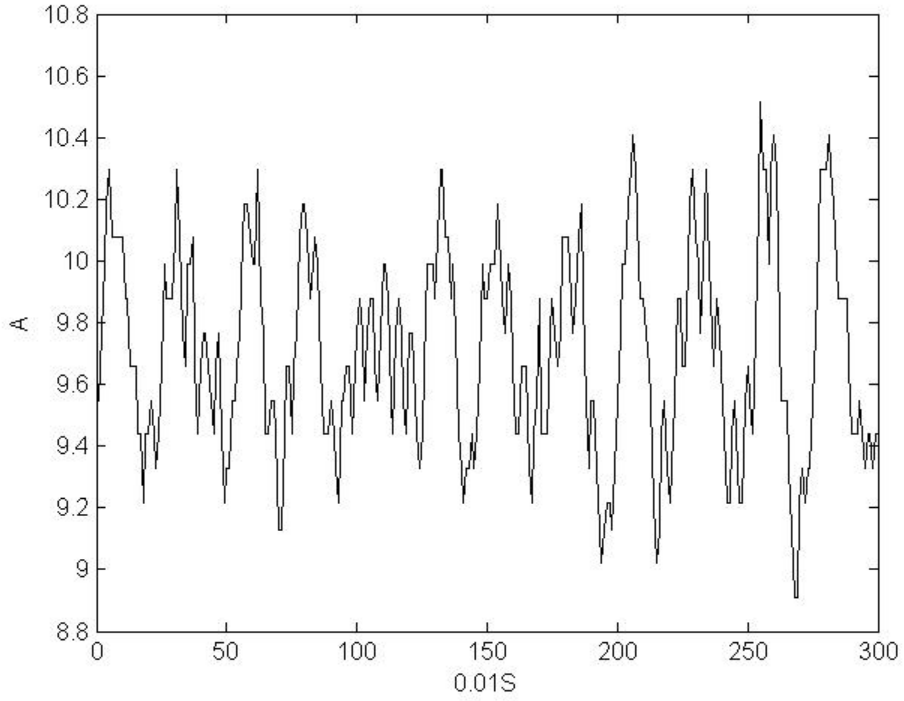

Figure 4.22 The direct current of experiment with no hammer form experiment

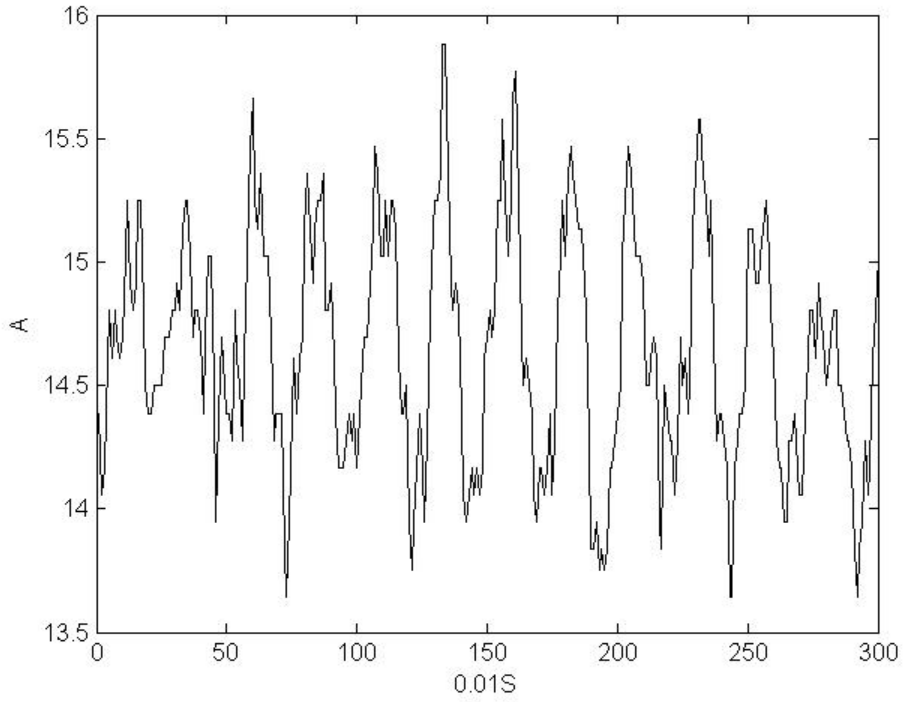

Figure 4.23 The direct current of experiment with the hammer form experiment

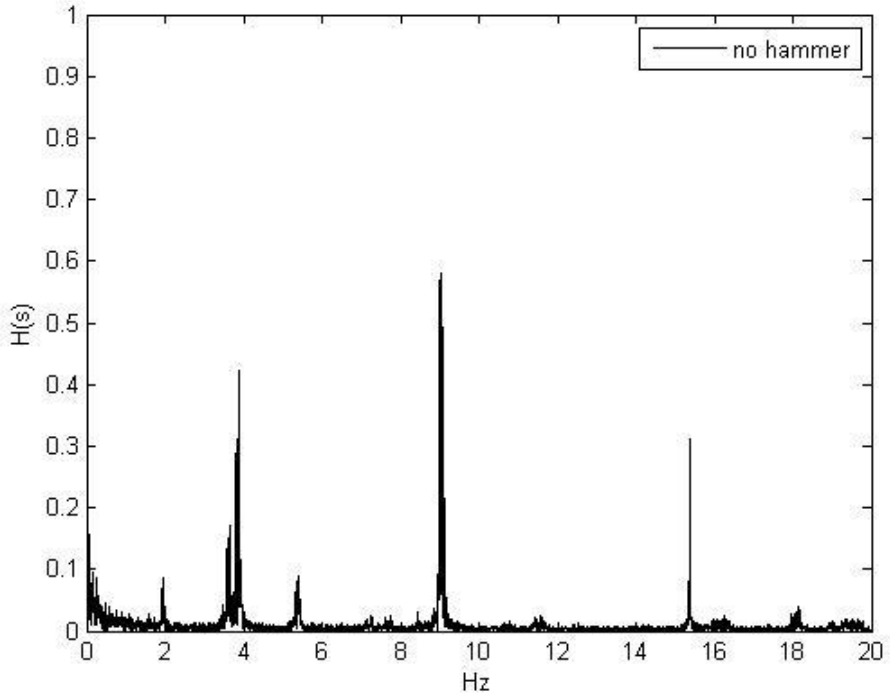

Figure 4.24 The FFT of the finite swing motion for the experiment with no hammer

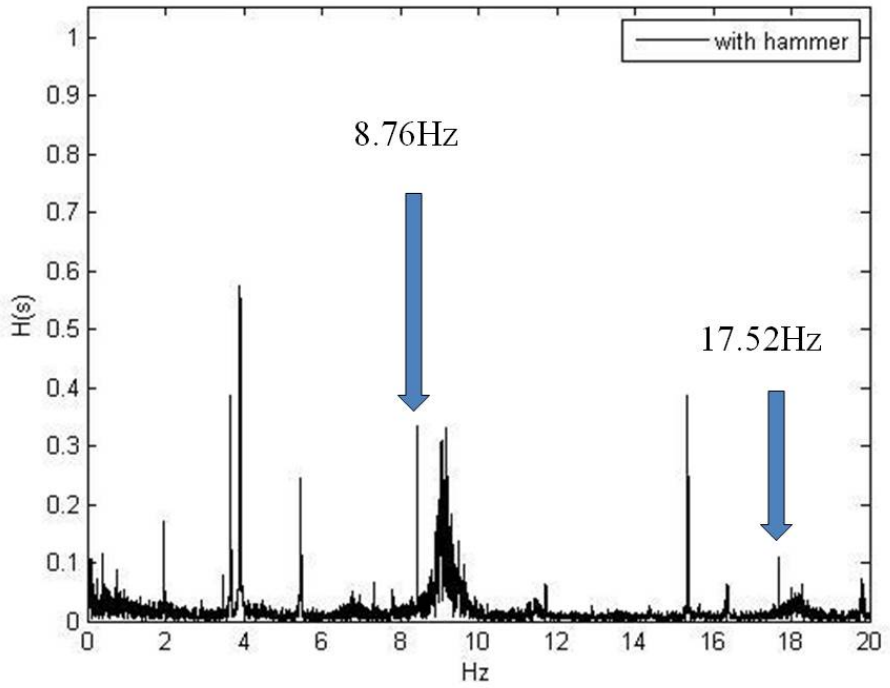

Figure 4.25 The FFT of the finite swing motion for the experiment with hammer

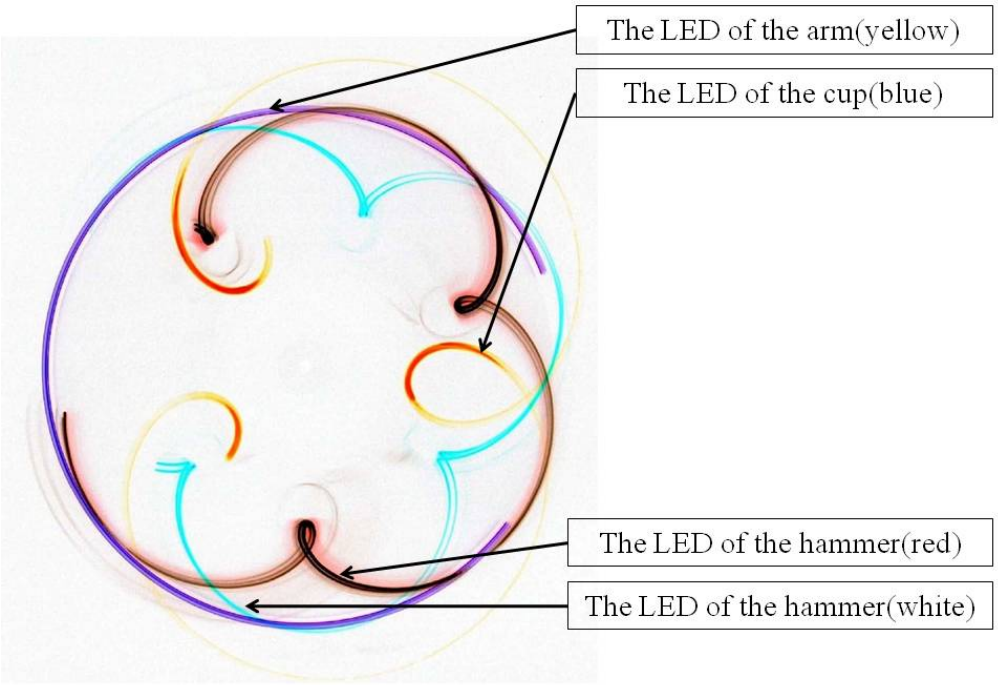

Figure 4.26 The louse of the finite swing motion form experiment

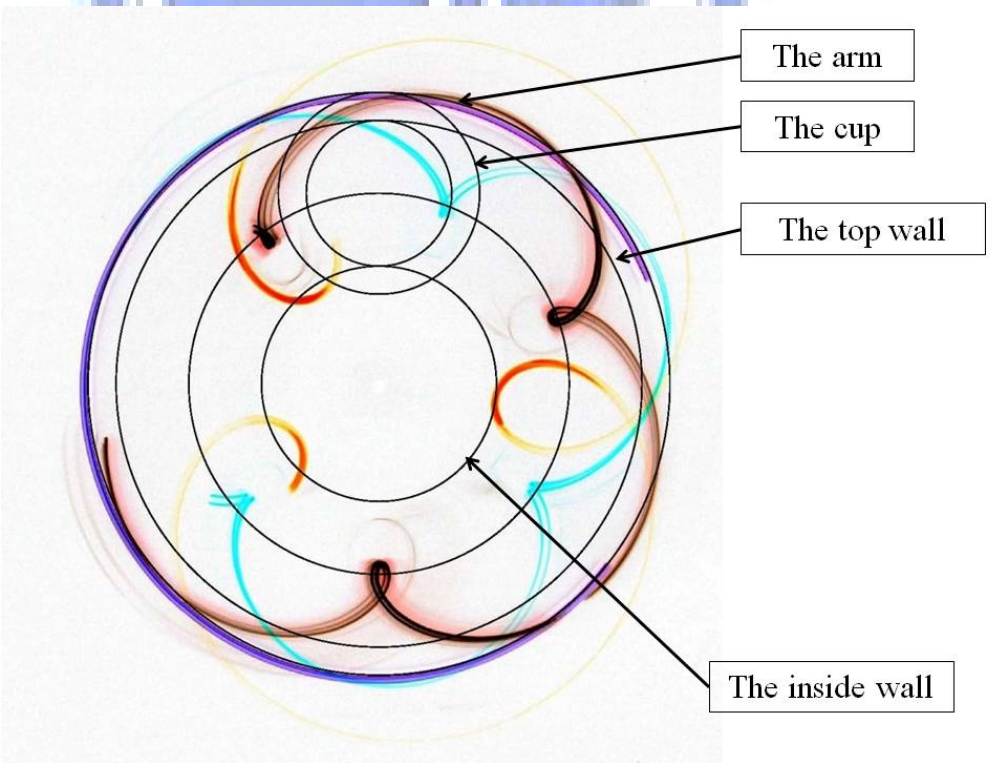

Figure 4.27 The top view on the louse of the finite swing motion form experiment

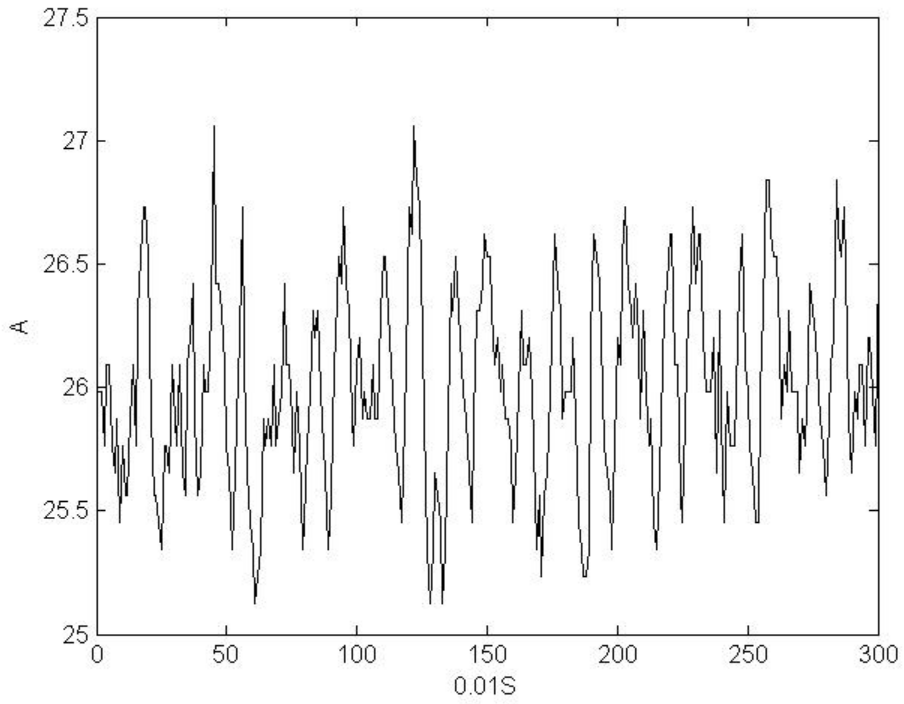

Figure 4.28 The direct current of the continuous rotation motion form experiment with no hammer

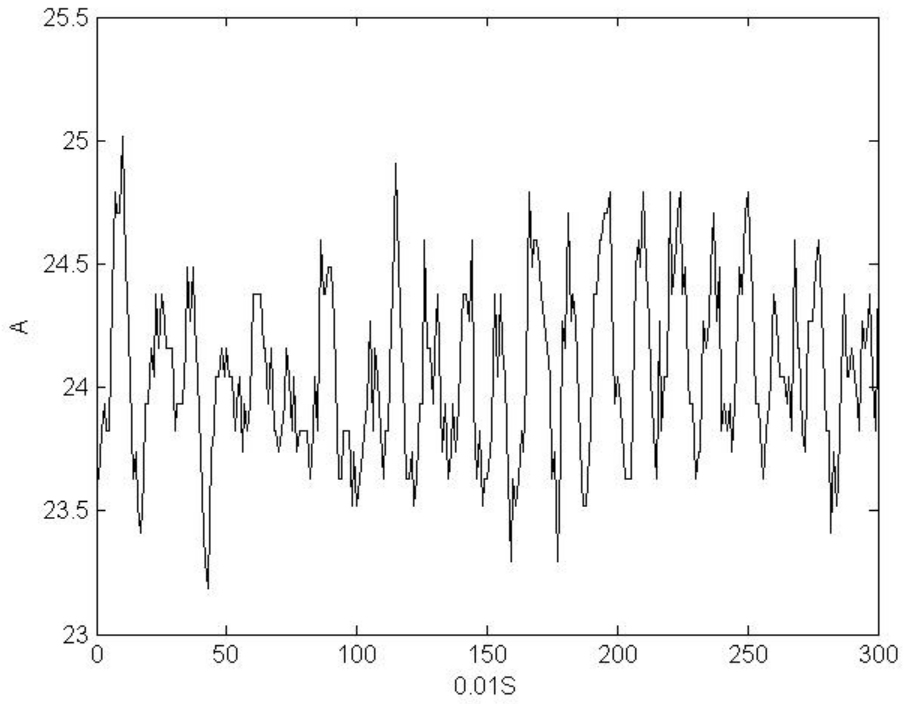

Figure 4.29 The direct current of the continuous rotation motion form experiment with the hammer

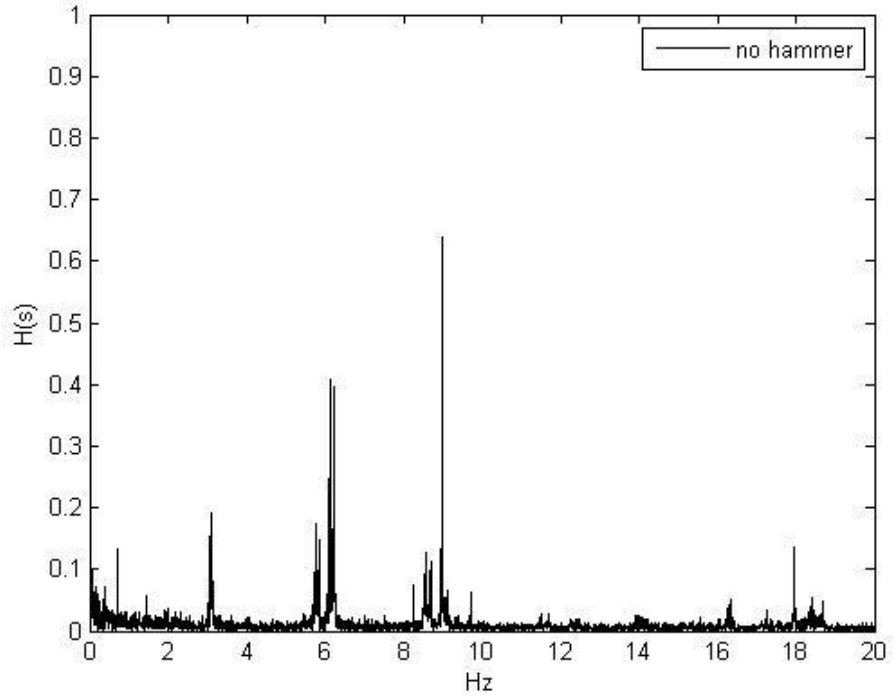

Figure 4.30 The FFT of the continuous rotation motion form experiment with no hammer

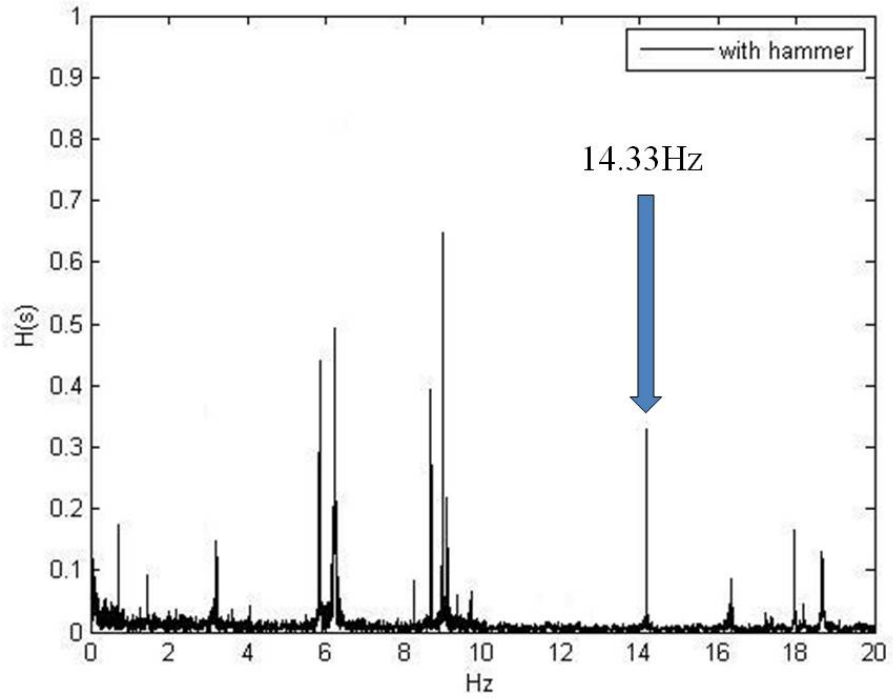

Figure 4.31 The FFT of the continuous rotation motion form experiment with the hammer

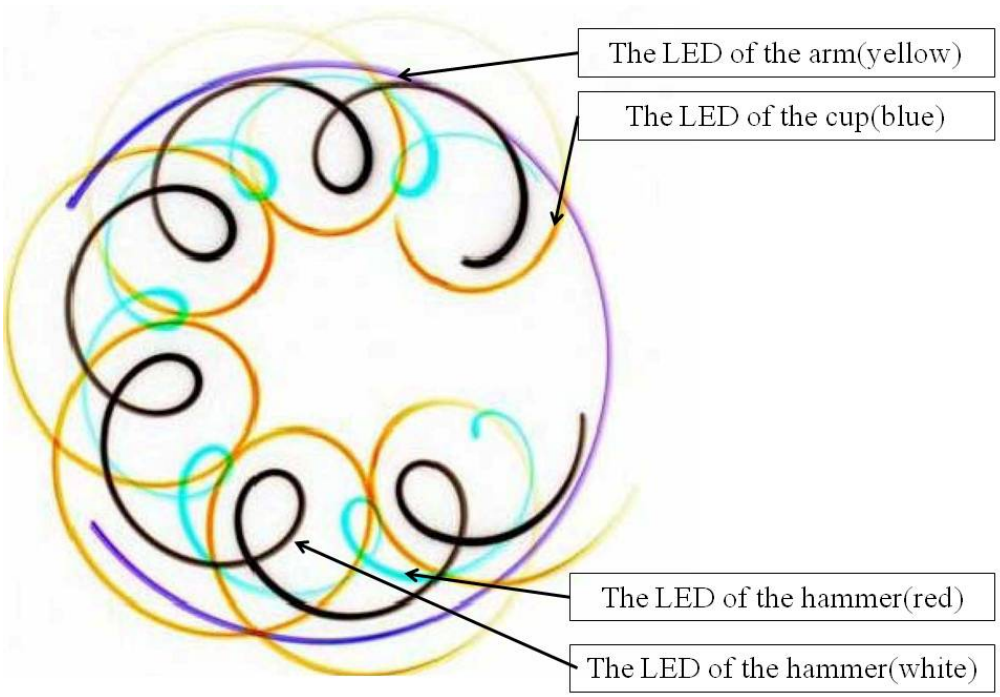

Figure 4.32 The louse of the continuous rotation motion form experiment

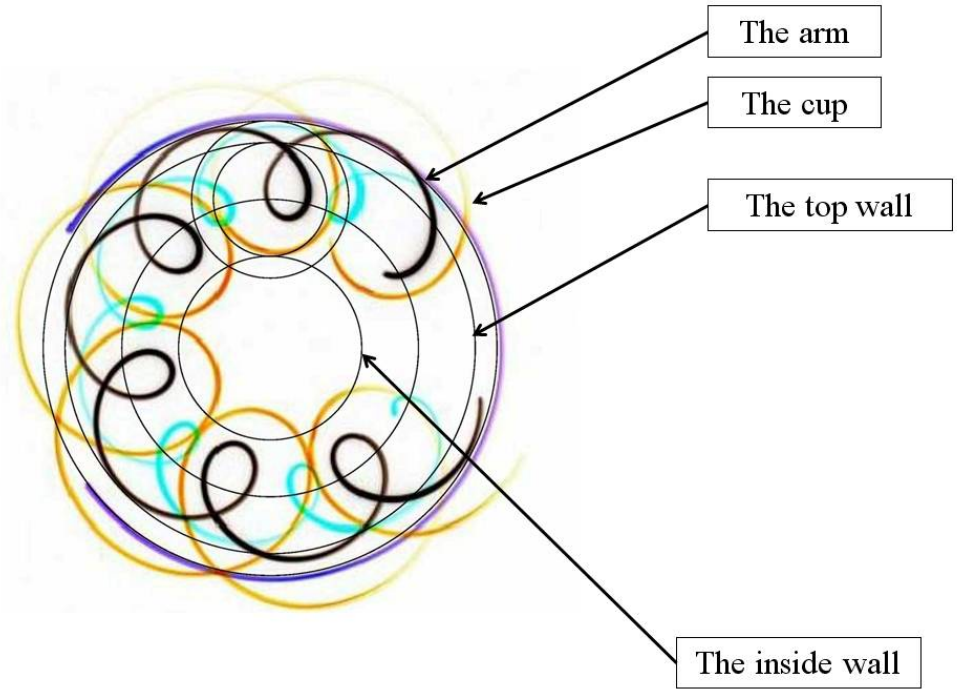

Figure 4.33 The top view on the louse of the continuous rotation motion form experiment